Anders Lund · Masaru Shiotani *Editors*

Applications of EPR in Radiation Research

Springer

Contents

Chapter 17
Study of Spin-Correlated Radical Ion Pairs in Irradiated Solutions by Optically Detected EPR and Related Techniques

Vsevolod Borovkov, Dmitri Stass, Victor Bagryansky and Yuriy Molin

Abstract The strong Coulomb attraction and recombination dramatically shorten the lifetime of radical ion pairs generated by ionizing irradiation in organic solutions, which complicates the use of conventional EPR spectroscopy to study these short-lived radical ions. However, the recombination of the oppositely charged ions gives birth to a fluorescence response of the irradiated media. This response appears to depend on the same properties of the radical ions that are studied by EPR spectroscopy. The dependence can be revealed with an external magnetic field, thus allowing a quantitative study of hyperfine couplings, spin-orbit interaction, paramagnetic relaxation times of radical ions, whose lifetime can amount to only a few nanoseconds. In this chapter we consider experimental approaches, both steady-state and time-resolved, which are based on the registration of the fluorescence response influenced by an external magnetic field. These are Optically Detected EPR, MARY (Magnetically Affected Reaction Yield) spectroscopy, and the technique of Time-Resolved Magnetic Field Effect (TR MFE) in recombination fluorescence. A brief history, a theoretical background, methodological details, as well as some unique experimental results obtained with these techniques are discussed.

17.1 Introduction

It is difficult to tell when the chemical effect of radiation on a molecular medium ends, but it begins at the moment when the radiation makes electrons leave the closed electron shells of the molecules forming (super)excited and ionized molecular states. Within several picoseconds a lot of species with open electronic shells appear in the region where an ionizing particle has passed. Some of them have electric charge, some are neutral. Although conventional EPR is generally sensitive to any paramagnetic species, in practice it is only applicable to study neutral radicals that

V. Borovkov (✉) · D. Stass · V. Bagryansky · Y. Molin
V. V. Voevodsky Institute of Chemical Kinetics and Combustion, SB RAS, 3, Institutskaya Str., Novosibirsk, Russia
e-mail: borovkov@kinetics.nsc.ru

V. Borovkov · D. Stass · V. Bagryansky
Novosibirsk State University, 2, Pirogova Str., Novosibirsk, Russia

A. Lund, M. Shiotani (eds.), *Applications of EPR in Radiation Research,*
DOI 10.1007/978-3-319-09216-4_17

escape from the track into the bulk with high probability. Radical ions arising as the pairs of oppositely charged species recombine quite quickly with their partners, with only few of them (several per cent in non-polar solutions) becoming separated by a very large distance. Thus, the Coulomb interaction and recombination dramatically limit the applicability of conventional EPR to study the radiation-generated radical ions in organic solutions.

In this chapter we discuss a somewhat different approach to study such radical ions. It is based on the spin correlation between the partners in a substantial fraction of the recombining radical ion pairs. Experimentally it can be implemented by detecting the luminescence response of the irradiated medium and investigating the effect of an external magnetic field on this response. In this chapter we discuss several ways to develop this approach, including Optically Detected EPR (OD EPR), MARY (Magnetically Affected Reaction Yield) spectroscopy, and the technique of Time-Resolved Magnetic Field Effect (TR MFE) in recombination fluorescence. All these methods share their basic principles with EPR and thus provide information similar to information obtained by magnetic resonance techniques: g-values, hyperfine coupling (HFC) constants, paramagnetic relaxation times of the recombining radical ions. For practical use it is important to realize that they have their own, often adjacent, but not fully overlapping, areas of optimal use.

The discussion is arranged as follows: first, we give a very brief historical overview, outline the basic principles of the approach, and provide an overview of the processes in the track of an ionizing particle where radical ion pairs arise and decay. Then, we discuss several key theoretical notions that the techniques rely upon, the experimental implementation of the techniques, and results obtained from the study of various radical ions, including many that were not studied by other techniques. This chapter mostly focuses on results obtained in this century.

17.2 Historical Sketch

The history of the controlled effect of radiation on the matter starts from the discovery of cathode rays [1], X-rays [2], and radioactivity [3]. These very discoveries and the active exploration of the properties of radiation became possible, to a large extent, due to the fact that the radiation-induced luminescence of matter is a widespread phenomenon that can be easily observed by eye.

In the beginning of the XX century it was realized that at least some part of the luminescence comes from the recombination of oppositely charged ions [4, 5]. A little later it was found that the recombination of ions in an irradiated matter can only be described if their pairwise generation is taken into account, which means that their initial spatial correlation is important [6]. Those days, the luminescence itself was interesting to the explorers of radiation primarily as an indicator of the presence of ionizing radiation or as a measure of certain atomic parameters. Only in the 1960-s it was understood that it was ion recombination that produced a considerable fraction of the luminescence response from irradiated organic solutions,

and that the ratio of singlet (S) and triplet (T) states of the excited recombination products was not statistical, i.e., it differed from S:T = 1:3 [7, 8].

In the milestone work [9] it was proposed that, due to the initial spin correlation in the primary pairs, the relation between the singlet and the triplet-excited states in radiolysis could change with time in a static external magnetic field or a resonance microwave field driving EPR transitions. An applied magnetic field modifies the proportion of singlet and triplet pairs, which was detected experimentally by Brocklehurst et al. [10] as an increasing yield of singlet excited states with a simultaneous decrease of the yield of triplet states. The variations of predicted magnetic field effects in time were found to depend on the hyperfine interactions in the radical ions [11, 12]. This opened the possibility to use the method of Time-Resolved Magnetic Field Effect (TR MFE) in recombination fluorescence to study the properties of the radical ions themselves, more specifically, those of them, whose recombination leads to the excited states of luminescent molecules. Quantum beats driven by the hyperfine interactions in the spin-correlated radical ion pair, the precursor of the excited molecule, were detected in the recombination fluorescence [13]. Very prominent quantum beats driven by the difference in the g-values of the geminate radical ions, the so-called Δg-beats, were also observed [14–16].

The dependence of the integrated yield of singlet excited states on the static external magnetic field strength—the so-called magnetic field effect curve—often has the form of a monotonously rising curve as the magnetic field strength is increased from zero to values much higher than the EPR spectrum width of the radicals [10]. However, it was found [17, 18] that features providing detailed information about both HFC in the radicals and their lifetimes appear in stationary MFE curve.

In 1979, the idea of the effect of the microwave field on the yield of singlet excited states was implemented in the optical detection of the EPR spectra of organic radical ions in a solution irradiated by continuous ionizing radiation [19, 20]. A year later, a time-resolved version of the EPR registration technique named Fluorescence Detected Magnetic Resonance (FDMR) was developed in Argonne National Laboratory (USA) based on a pulsed electron accelerator [21].

The OD EPR technique was used to study the primary charge carriers and the secondary radical ions in irradiated organic solutions [22–25]. Both the experimental method and the theoretical approaches were further developed. This considerably extended the range of objects studied by techniques, which focus on spin-correlated radical ion pairs generated in organic solutions by ionizing irradiation.

17.3 Track Structure and Spin-Correlated Radical Ion Pairs

After an ionizing particle passes through an organic medium, within several picoseconds primary ion pairs are formed consisting of a radical cation (hole) of the matrix/solvent and an excess electron. The ejected electron reaches thermodynamic equilibrium with the medium at a distance of about several nanometers [26].

Typically, radical ion pairs (RIPs) do not arise as isolated objects, and there is a non-zero probability of recombination of the charged species produced by ionization of different molecules. Such RIPs are called non-geminate. It is usually assumed that their recombination produces excited singlet and triplet states in the proportion S:T = 1:3. On the contrary, geminate RIPs, originating from the same molecule, can exhibit a non-trivial evolution of the S:T proportion in time, since these RIPs are spin-correlated.

For the approaches discussed in this chapter it is essential that this evolution also depends on the external magnetic field. Thus, the magnitude of the TR MFEs related to spin-correlated RIPs depends on the ionization density. For solutions of aromatic luminophores, the typical TR MFE magnitude decreases from 40 % for irradiation with fast electrons to several per cent for irradiation with helium ions [27] in accord with the expected decrease in the fraction of singlet RIPs. In refs [28, 29] similar effect was observed on going from soft X-rays to fast electrons. The maximum amplitude of the TR MFE curves in recombination fluorescence—up to 80 %—was observed under synchrotron radiation with quantum energy 15 eV [30]. For 40 eV quanta the effects were comparable to β-electron irradiation, decreasing to about 40 %.

A quantitative comparison of the local structure of the radiation track and the degree of the manifestation of spin correlation between the recombining ions can only be performed using computer simulation of the intra-track processes [31–33]. In particular, such simulations show that the ratio of the recombination rates for geminate and non-geminate RIPs in low viscosity liquids only weakly depends on time already after several nanoseconds.

17.4 Theoretical Background

Although the theoretical basis of the method of optically detected EPR is similar to conventional EPR, the application of the other two techniques, TR MFE and MARY, required an essential development to study the spin-correlated RIPs. The principles of spin effects in the reactions of species with open electronic shells were discussed in many works, including several reviews and monographs (e.g., see [34–38] and references therein). The experiments discussed in this chapter are focused on radical ions in non-polar solutions, and the measured value is the fluorescence intensity from the singlet-excited recombination products of RIPs. Such products are believed to arise from the recombination of RIPs in singlet spin state. Any phosphorescence generated upon the recombination of triplet pairs in solutions is either strongly quenched or can be rejected with an optical filter.

Thus, the intensity of the recombination fluorescence $I(t)$ is generally determined by the recombination kinetics $F(t)$ and the singlet state population $\rho_{SS}(t)$ of the radical ion pairs. Importantly, in non-polar solutions the Coulomb interaction is likely to result in equally effective recombination from both singlet and triplet states, independently on the magnetic field. Therefore, for RIP recombination in non-polar

solvents *F(t)* and $\rho_{SS}(t)$ are believed to be independent, and the experimentally observed kinetics *I(t)* is given by a convolution involving their product. At any rate, there is no known experimental evidence that contradicts this statement. For a short fluorescence time of the luminophore the convolution turns into a simple product, and *I(t)* can be represented as follows:

$$I(t) \propto F(t) \cdot \rho_{SS}(t). \tag{17.1}$$

This relationship in turn lets us separate the problem of describing the RIP spin dynamics from the very sophisticated task of calculating the time dependent yield of singlet excited molecules. In this chapter, the Time-Resolved Magnetic Field Effect (TR MFE) is defined as the ratio:

$$\frac{I_B(t)}{I_0(t)} \approx \frac{\rho_{ss}^B(t)}{\rho_{ss}^0(t)}. \tag{17.2}$$

The subscript and superscript *B* or 0 correspond to the measurements in high or zero magnetic field, respectively.

17.4.1 Evolution of Spin State of Spin-Correlated Radical Ion Pairs

In terms of spin chemistry, the evolution of an ensemble of RIPs proceeds as transitions between S and T states of the pair of unpaired electron spins of the radicals. The quantum beats between these states are driven by various interactions the two electron spins experience. These are, first of all, the interactions with external magnetic fields, either static or oscillating, and HFC with the magnetic nuclei of the radical ions. The interactions between the electron spins of the two organic radicals in a RIP are quite weak and can be neglected. Indeed, the exchange interaction has no effect for a RIP in non-polar solution, as the pairs mostly recombine from a distance of at least 10 Å [39] where these interactions are negligible. Also, due to the fast rotation of radicals in solution, only the isotropic components of both the hyperfine and g-tensors in each radical need to be considered. The fluctuating anisotropic components of the couplings can be accounted for as a contribution to paramagnetic relaxation.

Dynamics of Spin State of a Singlet Born RIP The results of the calculations can be most concisely presented using the density matrix $\hat{\rho}(t)$ of the spin system of the radical pair, as suggested by Schulten and Wolynes [40]. The population $\rho_{SS}(t)$ of the singlet electronic spin state can be obtained using the projection operator $\hat{P}_S = |S\rangle \langle S|$ applied to the density matrix

$$\rho_{SS}(t) = Tr\left\{\hat{P}_S \hat{\rho}(t)\right\}, \tag{17.3}$$

where *Tr* is the trace over the electron and nuclear indices. If there is no interaction between the electron spins of the radicals in the RIP, expression (17.3) can be written as

$$\rho_{ss}(t) = \frac{1}{4} + \sum_{i,k} T_{ik}^{(1)}(t) T_{ik}^{(2)}(t), \tag{17.4}$$

in terms of the components of the correlation tensor $T_{ik}^{(1,2)}(t)$

$$T_{ik}^{(1)}(t) = \left\langle Tr_e \left\{ \hat{S}_{1i}(t) \hat{S}_{1k}(0) \right\} \right\rangle, T_{ik}^{(2)}(t) = \left\langle Tr_e \left\{ \hat{S}_{2i}(t) \hat{S}_{2k}(0) \right\} \right\rangle. \tag{17.5}$$

Here, $i,k = \{x,y,z\}$, $\hat{\mathbf{S}}_{1,2}(t) = exp(i\hat{H}_{1,2}t)\hat{\mathbf{S}}_{1,2}exp(-i\hat{H}_{1,2}t)$ are the operators of the electron spins of the RIP partners in the Heisenberg representation, Tr_e is the trace over the electron spin variables, and the brackets mean averaging over the projections of the magnetic nuclei, H_1 and H_2 are the Hamiltonian terms (frequency units) for the interactions in each radical. This approach simplifies the solution of the quantum problem for two nearly isolated sub-systems whose initial state is entangled, and makes it possible to account for different types of interactions in the radicals.

An analytical expression for the components of the correlation tensor (17.5) only exists for several special cases. For an arbitrary magnitude of the magnetic field along the *z* axis, an exact solution of this problem has only been found for the simplest case of one magnetic nucleus with spin *I* and HFC constant *a* [41, 42]. In this case, the components of the tensor are:

$$T_{xx} = T_{yy} = \frac{1}{2}\mathrm{Re}\, h(t), T_{xy} = -T_{yx} = \frac{1}{2}\mathrm{Im}\, h(t), T_{zz} = \frac{1}{2} g(t), \tag{17.6}$$

where

$$g(t) = 1 - \frac{a^2}{2I+1} \sum_{m=-I}^{I} \frac{I(I+1) - m(m+1)}{\left(2R_m\right)^2} \left[1 - \cos\left(2R_m t\right)\right],$$

$$h(t) = \frac{1}{4(2I+1)} \sum_{m=-I}^{I} \left[\left(1+D_m\right)e^{iR_m t} + \left(1-D_m\right)e^{-iR_m t}\right]\left[\left(1+D_{m-1}\right)e^{iR_{m-1} t} + \left(1-D_{m-1}\right)e^{-iR_{m-1} t}\right].$$

Here the following notation was used:

$$2R_m = \sqrt{\omega_0^2 + a\omega_0\left(2m+1\right) + a^2\left(I+0.5\right)^2}, D_m = \frac{\omega_0 + a\left(m+0.5\right)}{2R_m}, \text{and} \omega_0 = \frac{g\beta B}{\hbar}$$

is the Larmor precession frequency of the electron spin in external magnetic field of strength *B*, β is the Bohr magneton, and $\hbar$ is the Planck constant.

In zero field, the tensor (17.6) becomes diagonal with the non-zero components equal to

$$T_{xx}(t) = T_{yy}(t) = T_{zz}(t) = \frac{4I(I+1)+3+8I(I+1)\cos(a(I+0.5)\cdot t)}{6(2I+1)^2}. \quad (17.7)$$

Expressions (17.6) and (17.7) can be generalized for the case of several magnetic nuclei with equal HFC constants. To this end, these expressions should be averaged over I, the total nuclear spin [42]. In zero field an analytical solution can be obtained, for example, for n spin ½ nuclei with equal HFC constants a [43]:

$$T_{xx}(t) = T_{yy}(t) = T_{zz}(t) = \frac{1}{6}\left[\frac{n+3}{n+1} + \frac{2n(n+2)}{n+1}\left(\cos\frac{at}{2}\right)^{n+1} - 2n\left(\cos\frac{at}{2}\right)^{n-1}\right]. \quad (17.8)$$

In the limit of strong field $B >> a_n$ an analytical solution exists for an arbitrary set of magnetic nuclei with spins I_n and HFC constants a_n, with the nonzero components of the tensor equal to

$$T_{zz} = \frac{1}{2}, T_{xx} = T_{yy} = \frac{1}{2}\cos(\omega_0 t)G(t), T_{xy} = -T_{yx} = \frac{1}{2}\sin(\omega_0 t)G(t),$$
$$G(t) = \prod_n \left[\frac{1}{(2I_n+1)} \times \sin\frac{a_n(2I_n+1)\cdot t}{2} \Big/ \sin\frac{a_n t}{2}\right]. \quad (17.9)$$

There is also an analytical solution at B = 0 [44], although a quite cumbersome one, for two magnetic nuclei with different HFC constants, which can be generalized for two groups of equivalent nuclei.

For many magnetically non-equivalent nuclei with different HFC constants the semiclassical approximation can be used [40]. In this approximation, in the limit of strong field $B >> \sigma$, where $\sigma^2 = 1/3 \times \sum_n a_n^2 I_n(I_n+1)$ is the second moment of the EPR spectrum of the radical, the function $G(t)$ in (17.9) takes the form

$$G(t) = \exp(-\sigma^2 t^2/2). \quad (17.10)$$

For zero field the semiclassical approximation gives:

$$T_{xx} = T_{yy} = T_{zz} = \frac{1}{6}(1+2C(\sigma t)), \text{where } C(x) = (1-x^2)\exp(-0.5x^2). \quad (17.11)$$

For an arbitrary magnetic field the expressions for the correlation tensor in the semiclassical approximation are quite cumbersome. These expressions were first provided by Bagryansky et al. [45].

Paramagnetic Relaxation In practice, it is also necessary to take into account paramagnetic relaxation. The simplest phenomenological way to take the relaxation into account is to multiply spin operators $\hat{S}_z(t)$ and $\hat{S}_{x,y}(t)$ by factors $\exp(-t/T_1)$ and $\exp(-t/T_2)$, respectively, where T_1 and T_2 are the longitudinal and the transverse paramagnetic relaxation times [46]. For zero field, assuming $T_1 = T_2 = T_0$, this gives

$$\rho_{ss}(0,t) = \frac{1}{4} + 3e^{-t/T_0} T_{zz}^{(1)}(t) T_{zz}^{(2)}(t). \tag{17.12}$$

For a strong field the expression for $\rho_{SS}(t)$ can be written in compact form using the functions *G(t)* determined by the relevant expressions (17.9) or (17.10):

$$\rho_{ss}(B,t) = \frac{1}{4} + \frac{1}{4}e^{-t/T_1} + \frac{1}{2}e^{-t/T_2} \cos(\omega_0^{(1)} - \omega_0^{(2)})t \cdot G^{(1)}(t) G^{(2)}(t). \tag{17.13}$$

Here $1/T_{0,1,2}$ is the sum of the corresponding relaxation rates of the two radicals.

Expressions (17.6–17.13) were derived for an isolated singlet-born RIP. In order to apply them for fitting the experimental TR MFE curves, it is usually assumed that the ensemble of RIPs in the track can be divided into two parts. One part consists of those RIPs that are singlet-born spin-correlated pairs, whose spin evolution obeys the above equations, while another part includes uncorrelated RIPs related to cross recombination. This picture is of course only approximate. It is generally not as easy as it might appear to distinguish between spin-correlated and non-correlated recombining ion pairs in an ensemble. Finer effects connected with the transfer of spin polarization between pairs can also be expected [47], although they have not so far been detected experimentally.

In this approximation, the total singlet spin state population of the RIPs is written as $\theta \cdot \rho_{SS}(t) + (1-\theta)/4$ [37], where θ is the fraction of spin-correlated pairs among all of the RIPs, which recombine at a given moment. Although this fraction should generally depend on time, it was demonstrated that for a radiation spur of moderate size it is almost independent on time after the first nanoseconds [32]. In this chapter θ is assumed to be constant.

Examples of TR MFE Curves Figure 17.1 shows several TR MFE curves, i.e., the ratios of singlet state populations (17.2), calculated using Eqs. (17.3–17.13), and several curves for two groups of spin ½ nuclei. Unresolved EPR spectra of the RIP partners with very different widths appear in the TR MFE curve as two different peaks (Fig. 17.1a) at *t*(ns) of about 9/σ(mT). The peaks disappear if paramagnetic relaxation is fast enough. If the EPR spectra of both partners are narrow, the rate of the singlet-triplet transitions caused by HFC and the rate of the increase in the TR MFE curve are low, letting observe the Δg-beats in a high enough field.

A HFC with magnetically equivalent nuclei manifests itself as periodic peculiarities with positions in time determined by the HFC constant (Fig. 17.1b).

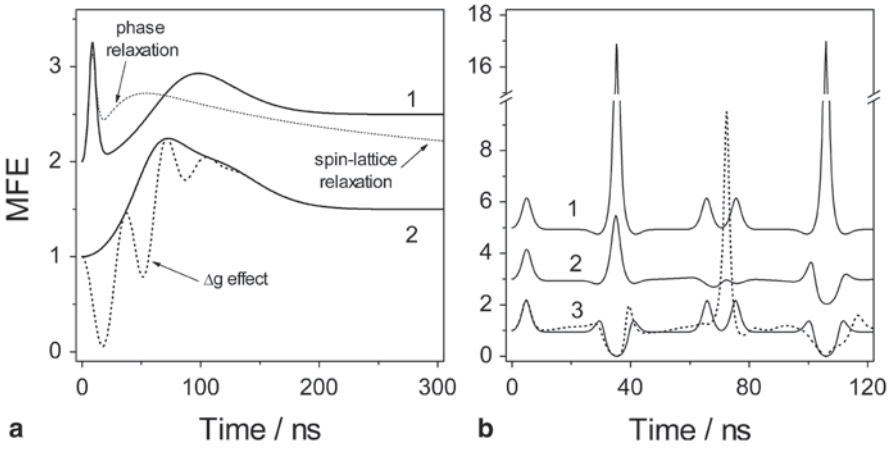

Fig. 17.1 Calculated TR MFE curves for a singlet-born (θ = 1) RIP composed of partners with equal *g*-values in the absence of paramagnetic relaxation (except as otherwise noted). The RIP partners are assumed to either both have unresolved EPR spectrum (**a**) or only one of them has non-zero HFC (**b**). Panel (**a**): $\sigma^{(1)} = 1$ mT, $\sigma^{(2)} = 0.1$ mT (*solid curve 1*); the same but $T_1 = 200$ ns, $T_2 = T_0 = 20$ ns (*dashed curve 1*); $\sigma^{(1)} = \sigma^{(2)} = 0.1$ mT (*solid curve 2*); the same assuming the difference of *g*-values $\Delta g = 0.002$ for the RIP partners at magnetic field $B = 1$ T (*dashed curve 2*). Panel (**b**): HFC constants with spin ½ nuclei $a(12H) = 1$ mT (*curve 1*); $a(12H) = 1$ mT, and $a(1H) = 0.5$ mT (*curve 2*); $a(13H) = 1$ mT (*solid curve 3*); $a(12H) = 1$ mT and $a(1H) = -1$ mT (*dashed curve 3*) calculated using the results reported in ref [44]

The presence of nonequivalent magnetic nuclei changes the relative amplitudes of the peculiarities, peaks or dips. The change also depends on the relative sign of the HFC constants, since the spin state evolution at $B = 0$ depends on this sign. A finite paramagnetic relaxation would result in the damping of the peculiarities with time.

The model presented above in Eqs. (17.3–17.13) can be applied with success to describe the experimental TR MFE curves. As an example, Fig. 17.2a shows TR MFE curves for RIPs that have magnetically equivalent nuclei only in one partner, either the radical anion or the radical cation, while the contribution of the other partner to HFC is negligible [42, 48]. Figure 17.2b shows a TR MFE curve for the RIP that is composed of these two radical ions, now both having HFC. A simulation shows that the maxima of the peaks correspond to the moments of time when the population of the singlet state in zero field is low. Since $\rho_{SS}(t)$ is determined by the product of contributions from each partner, the positions of the maxima in case (b) remain approximately the same. We also note that the amplitude of the experimental curve is lower as compared to the theoretical curves shown in Fig. 17.1, because in experiment $\theta < 1$ [29, 31, 33].

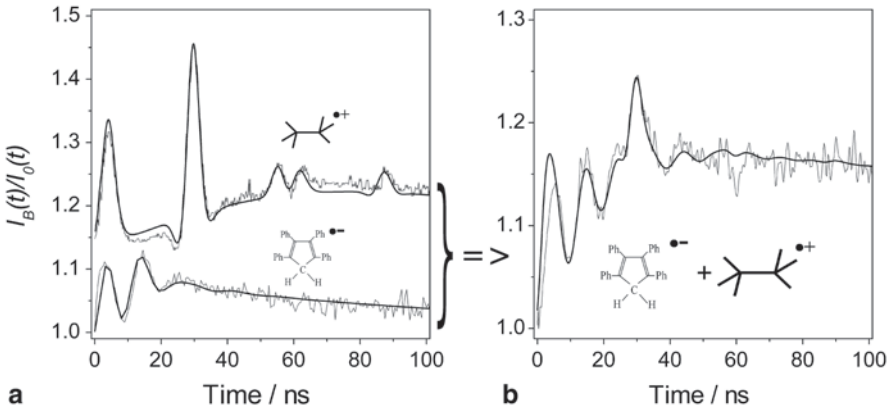

Fig. 17.2 **a** Experimental (noisy) and calculated TR MFE curves for solutions of 0.1 M hexamethylethane (+30 μM *para*-terphenyl-d_{14}) in *n*-hexane (*upper curve*, shifted by 0.15) ([42], adapted by permission of the PCCP Owner Societies) and 1 mM tetraphenylcyclopentadiene (TPCP) in *n*-decane (Adapted with permission from [48]. Copyright 1997, Mendeleev Communications). The *smooth lines* show the results of modeling for $a(18H) = 1.22$ mT (the radical cation of hexamethylethane) and $a(2H) = 2.5$ mT (the radical anion of TPCP). **b** Experimental (noisy) and calculated TR MFE curves for solutions of 0.1 M hexamethylethane +0.3 mM TPCP in *n*-octane (Adapted from Quantum beats in radical pairs. [38], Copyright 2007, Pleiades Publishing, Ltd). For both panels the temperature is 293 K, $B = 0.1$ T

17.4.2 MARY Spectroscopy

The expressions given above can be used to calculate the dependence of the recombination fluorescence intensity on the magnetic field strength in the conditions of continuous generation of radical ion pairs. Such dependences were named Magnetic Field Effect (MFE), or Magnetically Affected Reaction Yield (MARY) spectra (e.g., see [49–51]). For their theoretical description one has to calculate the integral yield of singlet states, *S(B)*, upon the recombination of RIPs:

$$S(B) = \int \rho_{SS}(t, B) \cdot F(t) dt \tag{17.14}$$

Even if *F(t)* is approximated by an exponential function, an analytical expression to describe the MARY spectra can only be obtained for the case of equivalent nuclei, Eq. (17.6). Using a more experimentally adequate non-exponential kinetics requires, in practice, a numerical simulation [52].

The left-hand part of Fig. 17.3 qualitatively shows a typical view of the signal in MARY spectroscopy, exemplified by the calculated function *S(B)*, for a pair with equivalent magnetic nuclei. When RIPs are generated in singlet spin state, one can always see a gradual increase of the luminescence intensity with the magnetic field, i.e., the so-called magnetic field effect. In zero field and in weak fields relatively sharp lines can also be observed where the energy levels of the radical ion pair cross

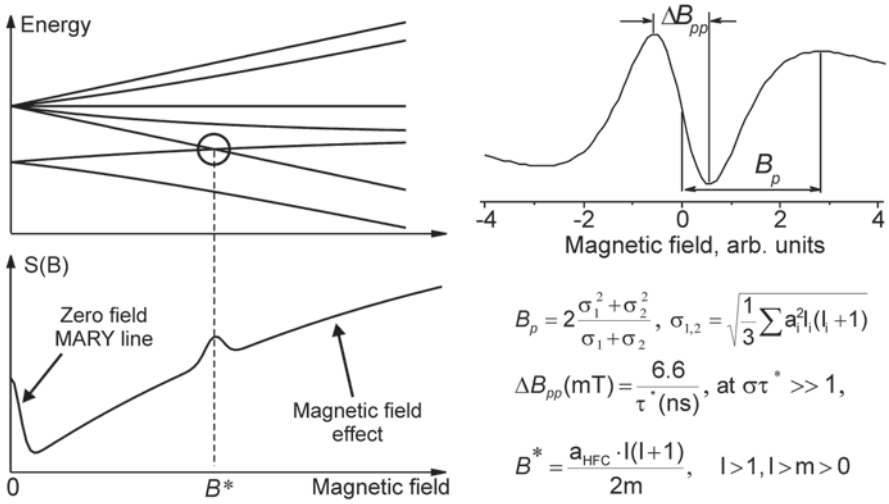

Fig. 17.3 A schematic diagram of the energy levels of a RIP and the field dependence of the singlet yield *S(B)* (*left*); a typical shape of the first derivative MARY spectrum (*right*) in the region of low magnetic field with indicated major features and their relation to the second moments of the EPR spectra σ^2, the lifetime of the spin correlated RIP τ^*, and to HFC constant, a_{HFC}, for the RIP with only equivalent nuclei in one of the partners. See text for more details

[41]. The lines appear due to the fact that for a part of the ensemble of RIPs the rate of singlet-triplet transitions drops as a result of destructive interference of several available transition channels. The zero-field line, also known as the MARY line or the Low Field Effect [53], is universal and appears in a wide range of systems [54–57]. This peculiarity appears due to a higher symmetry of the system in the absence of the preferred direction of the external magnetic field.

The right-hand part of Fig. 17.3 shows a characteristic view of the first derivative of the field dependence, *S(B)*, as obtained in the modulation experiment. The shape of this curve provides a quick estimate of the EPR spectrum width and the characteristic lifetime τ^* of the spin-correlated RIP. The former parameter is connected with the so-called magnetic field effect half-saturation width $B_{1/2}$ first suggested by Weller [58], which was later adapted to the more convenient in this setting position of the maximum in the modulation spectrum B_p [59, 75]. The time τ^* characterizing the overall rate of all processes shortening the lifetime of the spin-correlated state of the pair is connected with the width of the zero-field MARY line [41, 54, 60]. The connection between the width of the zero field line and the rate of decay of a spin-correlated RIP allows using the stationary MFE for estimating the rates of reactions involving short-lived radical ions (see below).

Additional lines can appear for radical ion pairs that have only equivalent nuclei in one of the partners (see also Fig. 17.5). They are observed in the fields that are the multiples of the HFC constant [49, 61]. Such lines in non-zero fields have also been observed for RIPs with a more complex HFC pattern [55]. Due to the presence of the additional lines in the MFE curve with positions determined by the

structure of the radical ions and with shape and width determined by the processes they are involved in, the observation of such effects evolved into a spectroscopy, and the curves are now referred to as MARY spectra [50]. The term MARY has been in use since the 1970s to refer to the studies of the static applied magnetic field in photogenerated radical pairs [62–64], however, it was radiation-generated RIPs that turned it into spectroscopy in the mid-1990s. The physical principles, typical experimental approaches, and a review of some results it has provided for radiation-generated pairs are discussed in detail elsewhere [49, 57].

17.4.3 Optically Detected EPR

In the technique of OD EPR the measured value is the intensity of recombination fluorescence *vs.* the external magnetic field in the conditions of continuous generation of RIPs and with applied microwave field. When the microwave quantum is in resonance with the energy difference between the Zeeman sublevels of the triplet state of a RIP, an additional depletion of the RIP singlet state occurs. The resonances thus observed via the decrease in the intensity of recombination fluorescence reproduce the EPR spectra of the radical ions composing the RIP. The theory of OD EPR [65–68] is similar to the theory outlined in Sect. 17.4.1, with a conversion to the frame of reference rotating with the microwave field frequency and using the strong field approximation valid for the region where the EPR resonances are actually located. Like in the case of MARY, the major difficulty in the quantitative simulation is the lack of information on the geminate recombination kinetics that needs to be convolved with the time dependent singlet state population. However, this uncertainty only affects the shapes of the lines in the described spectrum but not their positions.

At a low MW power OD EPR signals are very similar to the spectra observed in conventional EPR, but there are also some essential differences. One important peculiarity should be mentioned: a very short spin-lattice relaxation time, of the order of $T_1 \sim 10$ ns, makes the OD EPR line amplitude very small since the typical MW power (~ 1 W) cannot induce S-T transitions faster than the relaxation equilibrates the spin states. Increasing the MW power increases the signal but also results in a non-trivial saturation effect and a distortion of the OD EPR lines due to the so-called spin locking [69].

17.5 Experiment

17.5.1 Techniques

The Method of Time Resolved Magnetic Field Effects Figure 17.4 shows the experimental setup that was developed in the Institute of Chemical Kinetics and Combustion SB RAS (ICKC) [70] and provided most of the TR MFE data discussed

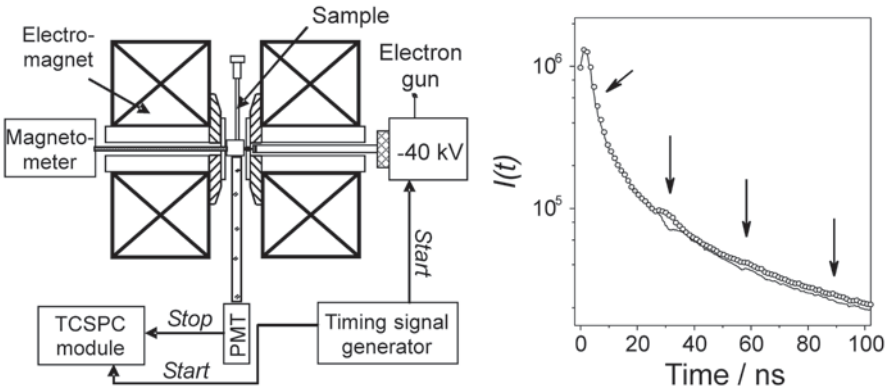

Fig. 17.4 A flow chart of the fluorimeter (*left*) and an example of the fluorescence decay kinetics (*right*) from an irradiated solution of 0.1 M hexamethylethane +30 μM *p*TP-d_{14} in *n*-hexane in magnetic field $B=0$ (*line*) and $B=0.1$ T (*circles*), T = 293 K. The *arrows* show the positions of the features arising in the TR MFE curve (see Fig. 17.2)

in this Chapter. The fluorescence is generated by short—about 1.5–3 ns—X-ray pulses with a characteristic energy of about 20 keV. This is mostly the characteristic radiation of a molybdenum target hit by a bunch of electrons with the energy of 30 to 40 keV. The bunch is guided through a hole in the electromagnet pole to the target located 20 mm away from the irradiated sample, which is positioned between the poles of the electromagnet. The fluorescence is registered by the Time-Correlated Single Photon Counting (TCSPC) technique. The magnetic field at the sample can be controlled in the range of 0–1.9 T.

As an example of the kinetics registered using this setup, Fig. 17.4 shows a raw kinetic curve of the fluorescence intensity decay for a solution of 0.1 M hexamethylethane +30 μM *para*-terphenyl-d_{14} (*p*TP-d_{14}) in *n*-hexane. The radical cation of hexamethylethane has HFC with 18 equivalent protons, which results in the pronounced quantum beats. Although the shape of the kinetic curve itself only allows this kind of conclusion to be made for the features at 30 ns, Fig. 17.2 justifies that for a high enough operation stability the coherent features can also be observed at 90 ns. The damping of the beats is due to the contribution from the HFC in the *p*TP-d_{14} radical anion ($\sigma \approx 0.068$ mT) and to phase relaxation.

MARY Spectroscopy To record a MARY spectrum, the static magnetic field at the irradiated sample has to be swept within several tens of mT through the zero of the field. To increase sensitivity, as in conventional EPR, lock-in detection with modulation of the swept magnetic field is used. In contrast with the standard magnetic resonance techniques, no microwave power is applied to the sample. Figure 17.5 shows a flow chart of the setup built in ICKC based on a commercial Bruker ER-200D EPR spectrometer [49]. A sample placed in the cavity of the EPR spectrometer is irradiated by an CW X-ray tube. The external magnetic field is generated by the magnet of the spectrometer, and its modulation coils are used to modulate the applied field at 12.5 kHz. To sweep through the zero of the field, a constant "nega-

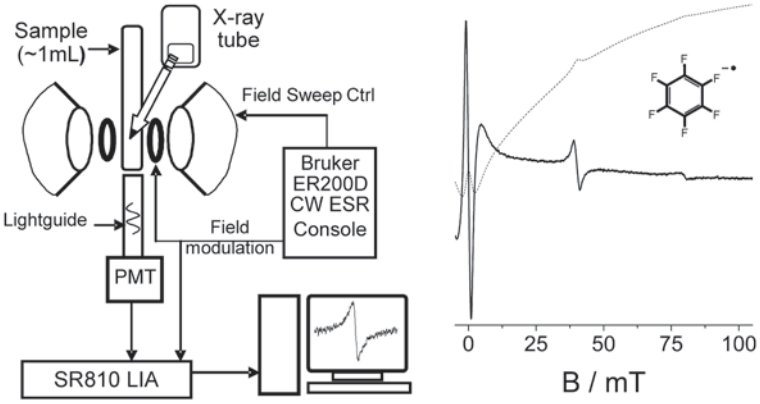

Fig. 17.5 A flow chart of the MARY spectrometer (*left*) and an example of a MARY spectrum registered as the first derivative for a solution of 10 mM C_6F_6 and 1 mM *p*TP-d_{14} in *n*-decane (*noisy line*) and the corresponding *S(B)* dependence shown by the dashed line (*right*)

tive field shift" is applied by an additional coil. The PMT signal at the modulation frequency is recovered by an SR810 lock-in amplifier.

The right panel of Fig. 17.5 shows an example of a first derivative MARY spectrum with all the possible features: the MFE signal appearing as a curve with a maximum around 5 mT, a strong zero-field line in the phase opposite to the MFE in the first derivative, and the extra lines in the fields ≈40 and ≈80 mT due to the presence of six equivalent nuclei with a HFC constant of 13.7 mT in the C_6F_6 radical anion.

MARY spectroscopy proved to be a helpful indicatory express technique to study the extremely short-lived radical ions with lifetimes down to 1 ns and their fast reactions. Its ease of use and short-time sensitivity balances the loss of the structural information, and thus this method complements the more powerful TR MFE and OD EPR techniques that are more demanding to the conditions of observation of the radical ions.

Optically Detected EPR The OD EPR spectra presented in this work were registered on the same setup described in the previous Section. The differences were that the sample was additionally exposed to a microwave field with a frequency about 10 GHz, and that the magnetic field was swept near the resonances located around 0.35 T [22, 71]. As can be seen in the examples below, the shape of the OD EPR spectra is similar to the shape of conventional EPR spectra.

A time-resolved version of the OD EPR technique was also developed using a pulsed electron accelerator [21, 72]. Here a pulse of the microwave field is applied to the sample with a controlled time lag after the irradiating pulse. Examples of the time-resolved OD EPR spectra can be found elsewhere [72–74].

Applications to Non-Alkane Solvents In most cases, the techniques discussed in this chapter have been applied to study radical ions in liquid alkanes. The advantages of alkanes, due to their low polarity, are the highest probability of the geminate ion recombination and the energy gain upon the ion pair recombination. The latter is due to the relatively low polarization energy of the recombining ions.

In other solvents certain obstacles could arise for applying a particular technique. Thus, the use of TR MFE is rather problematic in aromatic liquids, since aromatic molecules typically have a long fluorescence time, which distorts the pattern of the quantum beats. However, MARY and OD EPR can be readily used with these solvents [73, 75].

In ethers and alcohols a very fast deprotonation of the primary radical cations occurring within picoseconds is possible, leading to independent neutral radicals and cations and thus separating the spin and charge [76]. As a result, the newly formed ion pairs do not contain spin correlated electrons, and their recombination fluorescence is not magnetosensitive. However, magnetic resonance spectra of the radical ions of some aromatic solutes in liquid ethers and even alcohols can be detected using the recombination fluorescence [73]. Therefore, a portion of the delayed fluorescence from the irradiated solutions of aromatic compounds in these solvents comes from the recombination of spin-correlated radical ions of the solute molecules. Very recently [77] the precursors of aromatic radical cations were found in a series of ethereal solvents. So, the use of non-alkane solvents for the studies of magnetosensitive luminescence response of irradiated solutions is a subject of further work.

17.5.2 Experiment: Radical Anions

The mobility of electrons in alkanes is two to five orders of magnitude higher than the mobility of molecular ions. For concentrations of acceptors ~1 mM in liquid alkanes the radical anions (RAs) of the solute will quickly arise, while the solvent radical cations are not scavenged up to the times of the order of 100 ns (for viscosity ~1 cP). In these conditions, it is easy to study the contribution of RAs to TR MFE curves. Another way to study the radical anions is the use of a positive charge acceptor that does not scavenge the excess electrons in alkanes, like tetramethyl-*p*-phenylenediamine [78].

Radical Anions of Metaloles OD EPR and TR MFE were used to study RAs of tetraphenyl-substituted 1-heterocyclopenta-2,4-dienes (metaloles), siloles and germoles, including their chloro derivatives [79, 80]. Figure 17.6 shows the OD EPR spectra obtained for solutions of two of the studied compounds in a liquid alkane. The HFC constants were found to be about 1.5 mT for the two protons in the RA of compound (a) and 1.12 mT for ^{35}Cl in compound (b).

The TR MFE curves obtained in alkane solutions of the same compounds clearly demonstrate quantum beats induced by HFC in the RAs, which is dictated by the experimental conditions, as mentioned above. The dominant HFC constants in the RAs were determined from the simulation of the TR MFE curves. A very good agreement between the two techniques was achieved, thus indicating that in the OD EPR spectrum the same species are observed that are formed as early as few nanoseconds after the irradiation due to electron scavenging by the solute.

Radical Anions of Fluorobenzenes The RAs of fluorobenzenes were investigated in many studies (e.g., [81, 82] and references therein). They are interesting due to

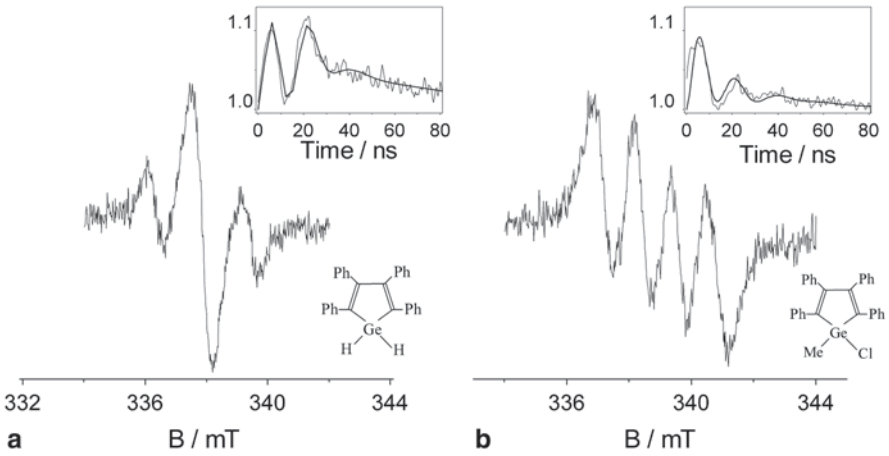

Fig. 17.6 OD EPR spectra (adapted with permission from [80]. Copyright 1998, Mendeleev Communications) and TR MFE curves (in the inserts, [79]. Copyright 1998, with permission from Elsevier BV) for solutions of compounds shown in the plots in liquid alkanes

their special electron and spatial structure. The HFC constants in these RAs are abnormally high because the flat molecular structure is disturbed by pseudo Jahn-Teller distortions in RAs [83]. The adiabatic potential energy surface (PES) for these RAs is a surface of pseudorotation with several minima. The motion along the pseudorotation trough modulates the HFC constants for the fluorines.

Because of their short lifetimes in solutions, these RAs cannot be studied using conventional EPR, but can be detected by OD EPR [84]. In particular, a nontrivial case of intra-molecular dynamics in a fluorobenzene RA was investigated in ref [85], where the OD EPR spectrum of the 1,2,3-trifluorobenzene (1,2,3-TFB) radical anion in a liquid squalane solution was registered (Fig. 17.7a).

The relatively high accuracy of measuring the HFC constants allowed detecting and analyzing the temperature dependence of the observed HFC. In Fig. 17.7b the experimental results are compared with the quantum chemical predictions. The predicted HFC constants were calculated by averaging in the model of fast exchange between the conformations along the pseudorotation trough. The relative weights of the conformations were estimated by the classical Boltzmann distribution, which gave a good agreement between the experiment and theory. Similar results were also obtained for the RAs of several other fluorobenzenes [86].

Symmetric 1,3,5-Trifluorobenzene Among the partially fluorinated benzenes, 1,3,5-TFB is remarkable for its highly symmetric structure. Its RA remained unobserved for a long time. All attempts to register its EPR spectrum using matrix isolation [87] or OD EPR in low-temperature squalane solution [84] failed. The difficulties preventing the registration of the EPR spectra of 1,3,5-TFB RA were usually attributed to the fast spin relaxation due to Jahn-Teller effect in the RAs of aromatic molecules having at least a third order symmetry axis (e.g., see [88]).

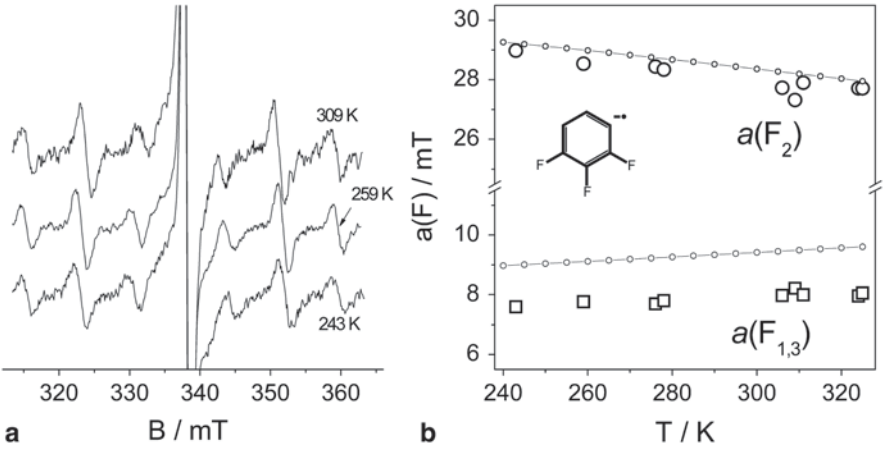

Fig. 17.7 **a** OD EPR spectra for a squalane solution of 10 mM 1,2,3-TFB (+1.5 mM *p*TP-d_{14}). Temperatures are given in the plot, **b** The temperature dependence of the experimentally measured averaged HFC constants (*open circles* for the fluorine atom in the second position (F_2) and *squares* for $F_{1,3}$) and the calculated results for this dependence in the quasi-classical model (-o-). Adapted with permission from [85]. Copyright 2005 American Chemical Society

The RA of 1,3,5-TFB was successfully registered in MARY experiments [89] in an alkane solution at room temperature. In theory the MARY spectrum of this radical anion should have a characteristic line in the field $15a_F/4$, where a_F is the HFC constant with the three equivalent fluorine nuclei. Indeed, a spectrum of this type was registered in a solution of 1,3,5-TFB in *n*-dodecane (Fig. 17.8a, the feature is shown with arrow), and its fitting provided the first estimate of the HFC constant of the ^{19}F nuclei in this RA.

OD EPR was also successful in registering the RA of 1,3,5-TFB [90]. The HFC constants with three equivalent ^{19}F nuclei in this RA estimated from MARY and OD EPR spectra are consistent and equal to $a(3F) \approx 7.4$ mT. Quantum chemical calculations predict a fast intramolecular exchange between the non-planar structures of this RA, thus confirming the observed equivalence of the fluorine nuclei. The lifetime of the spin-correlated state of the radical ion pair involving the 1,3,5-TFB RA was estimated from the width of the MARY line as ~20 ns.

Radical Anions of Al, Ga and In *tris*-8-Oxyquinolinates Radical ionic states not only play an important role in chemistry, they are also critical for modern molecular electronic devices including organic light-emitting diodes (OLEDs). OLEDs are multi-layer heterogeneous films capable of emitting light when an electric current passes through them. Here, the layers of coordination compounds such as aluminum *tris*-8-oxyquinolinate (Alq_3) functioning as electron transport and electroluminescent layers are important. The charge transport proceeds via the formation of radical ionic states of the coordination compounds, while their recombination is the source of the optical emission of the device. Studying the properties of their isolated radical ions in model systems can help understand the potential ways to improve these

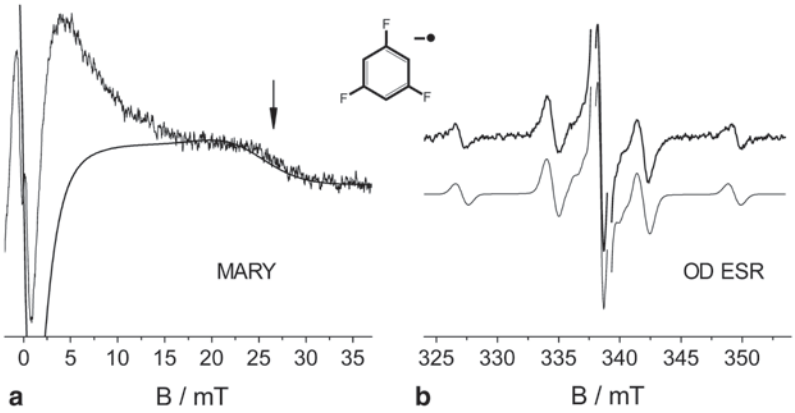

Fig. 17.8 **a** A MARY spectrum of a solution of 10 mM 1,3,5-TFB (+1 mM *p*TP-d_{14}) in *n*-dodecane and the results of fitting for a radical ion pair with a dominant HFC at three equivalent spin ½ nuclei with $a = 7.3$ mT. The difference between the predicted and the experimental spectra is due to the additional signal from pairs "solvent RC/*p*TP-$d_{14}^{-\bullet}$" [89], **b** An OD EPR spectrum of a solution of 10 mM 1,3,5-TFB (+1.5 mM *p*TP-d_{14}) in squalane at 309 K. The smooth line shows the fitting with $a(3F) = 7.4$ mT, $g = 2.0039$ in the radical anion. Reprinted from [90]. Copyright 2013, with permission from Russian Chemical Bulletin

electro-optical systems. As a system of this type, an X-irradiated solution of Alq_3 (as well as Inq_3 and Gaq_3) in benzene was used [75]. MARY spectra of radical ion pairs involving the RAs of the corresponding oxyquinolinate were successfully registered in these conditions, and their simulation provided the estimates of the HFC constants at the metal center (Fig. 17.9).

Experiments in liquid benzene demonstrated that the observed signal is produced by a pair consisting of the Mq_3 radical anion and the solvent radical cation narrowed by degenerate charge exchange. The registered MARY spectra are typical of a series of systems with a similar structure and demonstrate an increase in the second moment of the EPR spectrum of the pair partner with the dominant HFC, which in this case is the RA of the corresponding oxyquinolinate. Since all these three coordination compounds have the same number of identical ligands, the different behavior of the MFE is due to the different nature of the central ion. The shown spectra were simulated in the approximation of exponential distribution over the coherent lifetime of the pair, considering only one nucleus with the spin of the central metal ion in the radical anion ($I(^{27}Al) = 5/2$, $I(^{70}Ga) = 3/2$, $I(^{115}In) = 9/2$), the EPR spectrum width of the geminate pair partner, the benzene radical cation, could be neglected.

17.5.3 Experiment: Radical Cations

As mentioned above, in alkane solutions the secondary radical cations (RCs) are usually formed later than the RAs due to the very high electron mobility in these solvents. This significant time delay makes the techniques of TR MFE and MARY

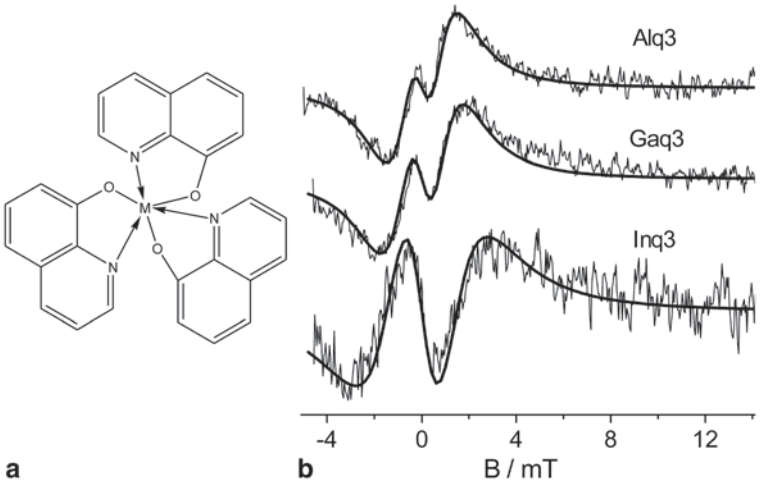

Fig. 17.9 **a** The structure of *tris*-8-oxyquinolinate M(III), where M = Al, Ga, In, (Mq_3). **b** Peak-to-peak normalized MARY spectra of benzene solutions of 1 mM Al, Ga, In *tris*-oxyquinolinates with superimposed simulated spectra with the following parameters: (Alq_3) a(I = 5/2) = 0.45 mT; (Gaq_3) a(I = 3/2) = 0.8 mT, (Inq_3) a(I = 9/2) = 0.6 mT. Reprinted from [75]. Registration of radical anions of Al, Ga, In tris-8-oxyquinolinates by magnetosensitive and spectrally resolved recombination luminescence in benzene solutions. Copyright 2012, with permission from Elsevier BV

virtually inapplicable to study RCs in diluted solutions, although still allows observing the secondary RCs using OD EPR. To observe the secondary RCs by TR MFE or MARY, either a higher concentration of the solute is required, or a solvent with a high mobility of the primary radical cations, like some cycloalkanes [91–93] or squalane [93], can be used. Molecules that cannot scavenge electrons are more convenient for the study of their radical cationic states. A luminophore giving a radical anion with a suitable HFC pattern can then be used as an electron acceptor.

The discussed techniques were used to study the RCs of a series of olefins [95, 96], aliphatic amines [97, 98], and aromatic compounds with negative electron affinity, like methyl substituted benzenes [99, 100]. This chapter focuses on the RCs of aliphatic hydrocarbons and their metalorganic analogues. For these compounds, the discussed techniques allowed obtaining EPR parameters of a series of their RCs in solution for the first time.

Data on Alkane Radical Cations from Other Techniques The RCs of alkanes, along with the excess electrons, are the primary species arising upon irradiation of alkanes in liquid or solid phase, and the history of their studies counts decades. The structural information on the RCs of alkanes was mostly obtained for low molecular weight (up to 8–10 carbon atoms) alkanes stabilized in low temperature matrices (e.g., see review [101] and references therein).

The RCs of normal, branched, and cyclic alkanes exhibit very different electron and spin density distributions. The ground states of both the neutral molecules of *n*-alkanes and their radical cations were found to be the elongated *all-trans* confor-

mation. In this conformation of the RCs the molecular orbital occupied by the unpaired electron embraces the entire carbon skeleton. The major HFC of the unpaired electron are observed for the two protons of the methyl groups located in the plane of the carbon skeleton. The value of the HFC constants decreases with increasing the skeleton length from ~10 mT (propane) to ~2 mT (*n*-decane).

In the RCs of branched alkanes the unpaired electron is mostly localized at one C-C bond, and thus more β-protons are involved in the hyperconjugation [101]. A typical value of the dominant HFC constants with the protons in the non-rotating methyl groups is 4–5 mT. The results from the studies of the RCs of cyclic and bicyclic alkanes in matrices (see, e.g., [102–104]) showed that many of them typically have several energetically close or identical structures with considerable HFC constants and substantially different distribution of spin density due to vibronic interaction [83].

Experiments on pulsed radiolysis of liquid alkanes demonstrated that the chemical lifetimes of the RCs of *n*-alkanes at ambient conditions should be in the range of several nanoseconds to several tens of nanoseconds [105]. For cyclohexane RC, numerous studies suggest that its lifetime in solution should be at least about a microsecond [92]. As for the RCs of branched alkanes, the usual techniques gave contradictory information on the lifetimes of the species in solution. In particular, in a study of neopentane and 2,2,4-trimethylpentane a hypothesis was put forward that these RCs transform into products in the sub-nanosecond time domain [106].

A study of the magnetic resonance parameters of alkane RCs in liquid phase became possible after the Optically Detected EPR and its time-resolved counterpart were developed. OD EPR was used to register the RCs of hexamethylethane, some cyclic alkanes with rigid structure like *cis*-decalin, norbornane etc. in solution [25, 71, 107]. As the solvent, alkanes with a higher ionization potential (cyclopentane, *n*-pentane, *n*-hexane) were usually used. OD EPR lines about 0.3 mT wide attributed to the solvent RCs were successfully observed in irradiated pentadecane and squalane [107]. The small EPR spectrum width was explained by the degenerate electron exchange involving the primary radical cation.

A considerable progress in the investigation of alkane RCs in solutions was made using the TR MFE technique. These results are discussed below.

Normal Alkanes In most cases the same approach was used to study alkane RCs in solutions: addition of the studied alkane (RH) in a concentration of 0.01 ÷ 1 M to an alkane with a higher ionization potential, usually *n*-hexane [108]. As the electron acceptor and luminophore, *p*TP-d_{14} at a low, 10-100 μM, concentration was used. Under these conditions the observed TR MFE is determined by spin evolution in the spin-correlated pairs ($RH^{+\bullet}$/*p*TP-$d_{14}^{-\bullet}$). The radical anion has small HFC constants, and its effect on the evolution of the RIP spin state becomes noticeable only at times longer than 50 ns.

Figure 17.10a shows TR MFE curves for solutions of *n*-alkanes at a relatively low concentration. A further increase in the *n*-alkane concentration modifies the curves as a result of slowing down the S-T transitions in the RIP due to the degenerate electron exchange, as discussed below. The shape of the curves clearly shows

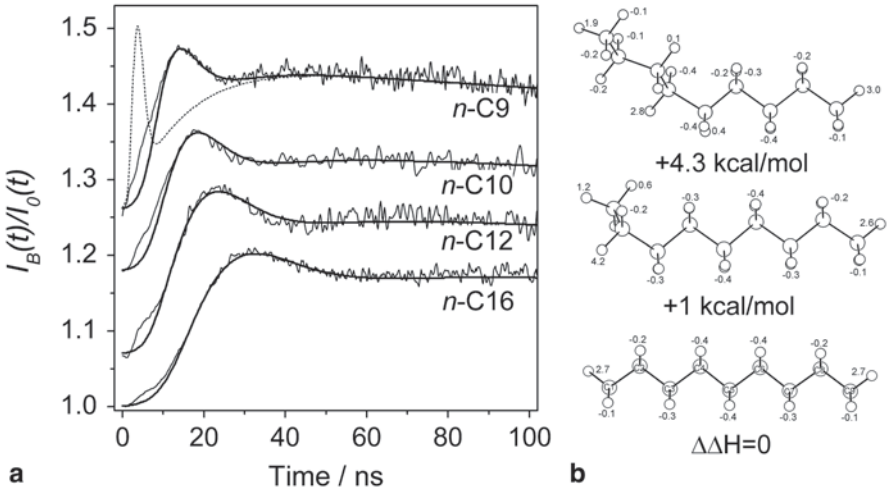

Fig. 17.10 **a** Experimental (*noisy*) and calculated TR MFE curves for solutions of 0.1 M *n*-alkanes (indicated in the plot) in *n*-hexane (+30 μM *p*TP-d_{14}) at 293 K. The *smooth lines* show the results of modeling with the second moment of the EPR spectrum of *n*-alkane RC corresponding to σ equal to 0.68, 0.5, 0.38, and 0.25 mT (C9–C16) in good accordance with data reported in Ref. [108]. For *n*-C9 the *dashed curve* demonstrates the change of the calculated TR MFE curve when σ is increased to 2.5 mT, which is typical for low temperature matrices [109]. **b** The *all-trans* structure of *n*-C9 RC and the conformations formed by rotation about either C_2–C_3 bond or C_4–C_5 bond by about 120°. The HFC constants with protons in mT and the relative values of the formation enthalpy as calculated by the UB3LYP/6–31G(d) method are also shown. Adapted with permission from [119]. Copyright 2006, American Chemical Society

that the RCs of *n*-alkanes with a sufficiently long carbon skeleton in solution have an unresolved EPR spectrum. A simulation of the TR MFE curves gives the σ values [108] for the EPR spectra from 0.81 mT (*n*-C8) to 0.25 mT (*n*-C16), which is much lower than the characteristic values for the spectra of the corresponding RCs in freon matrices. This is illustrated in Fig. 17.10a, where the experimental curves are fitted with Eqs. (17.10–17.13) taking the spectral exchange into account. For *n*-nonane solutions, a curve calculated for the value of σ typical for low temperature matrices is also shown with the dashed line. A small peculiarity at the time range <10 ns is likely due to the effect of the RCs of either the solvent or isomeric hexanes, for which σ values of about 2 mT were observed (see below).

The significant decrease in the EPR spectrum width of *n*-alkane RCs on going to liquid solution was explained in ref [119] using quantum chemical calculations. It was shown that in solution, similar to solid matrices, the most probable conformations of an *n*-alkane RC were the *all-trans* structure and the structure differing from it by rotation of the ethyl fragment, as demonstrated in Fig. 17.10b by the example of the nonane RC. The transition barriers between these conformations are only 23 kcal/mol [110]. The HFC constants are averaged not only by the fast rotation of the end methyl groups, but also by the rotation of ethyl fragments. Other conforma-

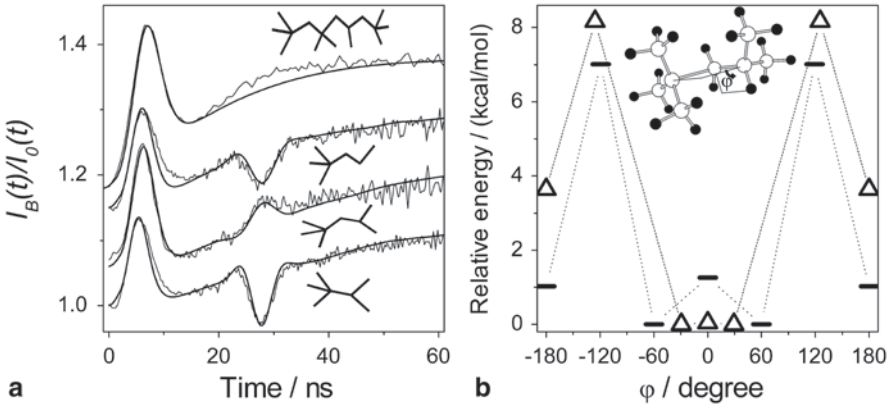

Fig. 17.11 **a** Experimental (noisy) and calculated TR MFE curves for solutions of 0.1 M branched alkanes (structures are indicated in the plot) in *n*-hexane (+30 μM *p*TP-d_{14}) at 293 K. Adapted with permission from [112]. Copyright 2012, American Chemical Society. The *smooth lines* show the results of modeling for the dominant HFC constants with β-protons of about 1.3 mT. **b** The relative energies of the stationary points at the energy profile for 2,2,4-trimethylpentane (*triangles*) and its RC (–) for the rotation about the C_3-C_4 bond. Adapted with permission from [111]. Copyright 2007, American Chemical Society

tions, even with a higher statistic weight, are unlikely to exist in solution due to high formation enthalpy.

Branched Alkanes The radical cations of branched alkanes were studied using the same approach as described above for normal alkanes. In this case, additional features (Fig. 17.11a) in the TR MFE curves appear indicating the presence of a significant number of magnetically equivalent protons with HFC constants of about 1.3 mT [111, 112]. This value is nearly equal to the HFC value expected for β-protons with the hyperfine couplings averaged by the fast rotation of the methyl groups. The change of the second feature from peak to dip for some compounds is due to the different parity of the number of protons with the dominant HFC in the corresponding RCs (see also Fig. 17.1b). Spin density in the RCs of isomeric butanes and pentanes is localized near the *tert*-butyl moiety. For higher substituted alkanes, such as 2,2,4,4,6,8,8-heptamethylnonane (Fig. 17.11a), the TR MFE curve becomes closer to the curve expected for a RC with a large number of magnetically non-equivalent nuclei (see Fig. 17.1).

In the RC of 2,2,4-trimethylpentane (Fig. 17.11b) for angle $\varphi \approx 180°$ the predicted HFC constant at the methine proton is about 7 mT. However, this large constant has no noticeable effect because in thermal equilibrium the parent neutral molecules mostly have conformations with $|\varphi| < 120°$. Since ionization is a vertical process, the RC appears in a similar geometry. A transition to the conformation with $\varphi \approx 180°$ required passing over a barrier of about 7 kcal/mol (Fig. 17.11b), which is unlikely at room temperature at times up to 50 ns where the quantum beats are observed. As one can see in Fig. 17.11a, a calculation neglecting the above conformation at $\varphi \approx 180°$ adequately describes the experiment.

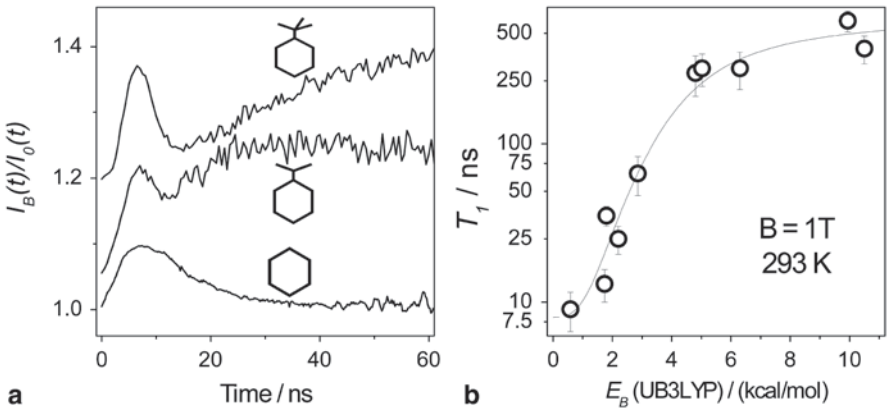

Fig. 17.12 **a** Experimental TR MFE curves for solutions of 0.1 M cyclic alkanes (structures are indicated in the plot) in *n*-hexane (+30 μM *p*TP-d_{14}) at 293 K. **b** The correlation between the pseudorotation barrier height E_B according to B3LYP calculations and the spin-lattice relaxation time T_1 of cycloalkane RCs (in the order of increasing E_B: cyclohexane, *trans*-decalin, ethylcyclohexane, 1,4-dimethylcyclohexane, methylcyclohexane, propylcyclohexane, *iso*-propylcyclohexane, 1,1-dimethylcyclohexane, 1,2-dimethylcyclohexane, *tert*-butylcyclohexane, *cis*-decalin). The *smooth line* is given as an eyeguide. Reprinted with permission from [115]. Copyright 2012, American Institute of Physics

The studied RCs were identified by the values of the HFC with protons and the *g*-values (~2.0035). Additionally, to check that the observed RCs are not the products of the possible decomposition of the parent alkane RC due to elimination of dihydrogen, TR MFE experiments for solutions of the corresponding alkenes were also performed. All these experiments confirmed that TR MFE allows registration of RCs of branched alkanes in solution and established that the lifetime of these RCs in solution at room temperature is at least tens of nanoseconds.

Cyclic Alkanes The RC of cyclohexane was probably one of the most elusive species that was sought by OD EPR in liquid solution. In pure cyclohexane the RC undergoes a fast degenerate electron exchange with the surrounding molecules, and it surely could be a precursor of the secondary RCs of solutes [15, 92, 113]. However, no signals were detected in the solutions where the cyclohexane RC was expected as an isolated species. A progress in studying this RC, as well as the RCs of alkylsubstituted cyclohexanes, was made using TR MFE, which allowed measurement of spin-lattice relaxation rates in these RCs.

As Fig. 17.12a shows, the features in the TR MFE curves reflecting the second moment of the EPR spectrum can only be observed if a bulky substituent like *tert*-butyl is present in the cyclohexane ring. In *iso*-propylcyclohexane, the effect of paramagnetic relaxation becomes more apparent as a faster decay of the TR MFE curve at longer times (see also Fig. 17.1a). In the RC of unsubstituted cyclohexane the time of spin-lattice relaxation in solution becomes so short (T_1 ~ 10 ns [114]) that this RC cannot be detected by OD EPR.

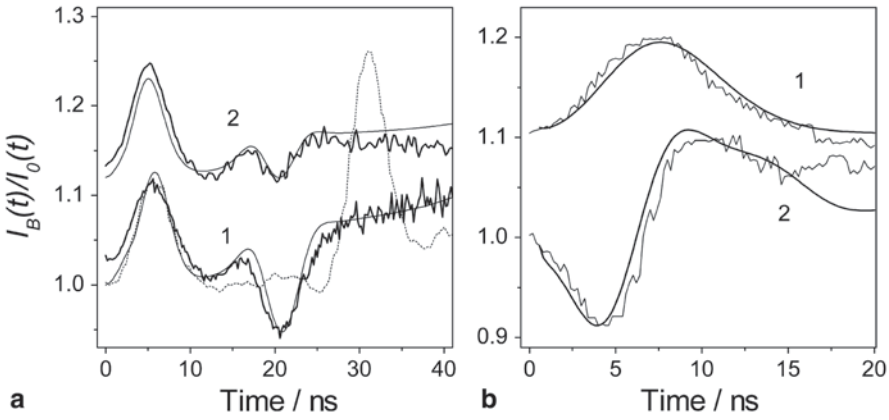

Fig. 17.13 Experimental (*noisy*) and calculated TR MFE curves obtained at 293 K for solutions of: **a** 0.1 M *tert*-butyltrimethylsilane (1) and *tert*-butyltrimethylgermane (2, shifted vertically by 0.12) in *n*-hexane (+30 μM *p*TP-d_{14}) at $B = 0.1$ T. The model curves correspond to two sets of HFC constants: $a(9H) = 1.87$ mT and $a(9H) \approx 0.3$ mT. The dashed line shows the experimental curve for a hexamethylethane solution in the same conditions. Reprinted from [117]. The study of radical cations of $Me_3C–SiMe_3$ and $Me_3C–GeMe_3$ in alkane solutions using the method of time-resolved magnetic field effect and DFT calculations. Copyright 2008, with permission from Elsevier; **b** 0.06 M solutions of Me_6Ge_2 (+30 μM *p*TP-d_{14}) in *n*-hexane at $B = 0.03$ M (*1*, shifted vertically by 0.1) and 0.3 T (2). The simulation parameters correspond to the data for RC of Me_6Ge_2 ($g \approx 2.03$, $a(18H) = 0.52$ mT [116, 118]. Adapted by permission of the PCCP Owner Societies)

Paramagnetic spin-lattice relaxation in the RCs of a series of cycloalkanes was analyzed from the viewpoint of the correlation between the relaxation rate and the structure of the adiabatic PES of the RCs [115]. The PES structure was obtained with DFT quantum chemical calculations. It was found that for RCs of all considered cycloalkanes, including alkyl-substituted ones, the corresponding adiabatic PES was a surface of pseudorotation due to avoided crossing composed of several minima on the PES separated by moderate potential barriers. A group of such minima forms a pseudorotation trough, along which the system moves without the rotation of the molecule. A correlation was revealed between the spin-lattice relaxation time and the calculated barrier height (Fig. 17.12b).

To explain the abnormally high paramagnetic relaxation rate in some cycloalkane RCs, it was proposed [115] that relaxation in radicals with nearly degenerate low-lying vibronic states originated from stochastic crossings of the vibronic levels caused by fluctuations of the radical interaction with the solvent. In the case of cyclohexane RC, an estimate for the relaxation rate derived using the Landau-Zener model of nonadiabatic transitions at the level crossing agrees well with the experimental data.

Radical Cations of Metalorganic Compounds Radical cations of aliphatic compounds with Group IV elements other than carbon were studied in alkane solutions using TR MFE [116, 117]. As an example, Fig. 17.13 shows TR MFE curves for solutions of *tert*-butyltrimethylsilane, *tert*-butyltrimethylgermane, and hexameth-

ylethane (a), and hexamethyldigermane (b), together with the results of fitting using the theory described in Section 17.4.1.

According to experimental data (Fig. 17.13a), when a metalorganic compound of the type $(CH_3)_3C–E(CH_3)_3$ (E = Si, Ge) is added to *n*-hexane, a positive charge carrier appears that has a considerably shifted *g*-value and a resolved EPR spectrum. In these RCs, the HFC constants are larger than in the RC of hexamethylethane (the dashed line in Fig. 17.13a). Using quantum chemical calculations this was explained by the shift of spin density at the C–E bond towards the carbon atom almost to equal extent in both compounds. As a result, the features in the TR MFE curves appear earlier than for hexamethylethane and change their sign because the number of nuclei with the dominant HFC constants becomes odd instead of even. The value of the HFC constants agrees very well with the calculations.

For compounds $(CH_3)_3E–E(CH_3)_3$ (E=Ge, Sn) the RCs are less stable in solution, although at sufficiently short times a positive charge carrier was observed with the second moment of the EPR spectrum and the g-value similar to those of $(CH_3)_3E–E(CH_3)_3^{\bullet+}$ observed in low temperature matrix, provided that the HFC constants are averaged by rotation of the methyl groups [116]. As Fig. 17.13b shows, the experimental curves are adequately fitted using the literature data.

The major qualitative result of the studies described in this Section is the estimation of the lifetime of the radical cations of aliphatic heteroorganic compounds in solution, which amounts to at least tens of nanoseconds.

17.5.4 Reactions of Radical Ions

Degenerate Electron Transfer An electron transfer between a radical ion and a molecule modifies the magnetic environment of the unpaired electron. This is also valid for the degenerate electron transfer, which we shall discuss in this Section using the example of an alkane RC reaction

$$RH^{+\bullet} + RH' \rightarrow RH + RH'^{+\bullet} \tag{17.15}$$

involving the molecules of an alkane added as a solute. In this reaction, the magnetic environment changes many times. The uncorrelated spectral exchange decreases the steepness of the TR MFE curve rise. This becomes readily detectable when the condition of the fast spectral exchange $(\sigma\tau_c)^2 << 1$ is met, as illustrated in Fig. 17.14a showing TR MFE obtained at various concentrations of *n*-nonane in *n*-hexane [119]. A simulation showed that the rate constant of reaction (17.15) for nonane is two orders of magnitude lower than the encounter rate for a radical cation and a molecule. The difference can be explained by assuming a noticeable probability of electron transfer in reaction (17.15) only if the *n*-alkane RC and its parent molecule are in the same conformation. As mentioned above, *n*-nonane RC can be found mainly in *all-trans* conformation, while the fraction of the appropriate conformations among the neutral nonane molecules in solution is quite low (~20 %). Another factor is the activation energy of the transfer (4–6 kcal/mol).

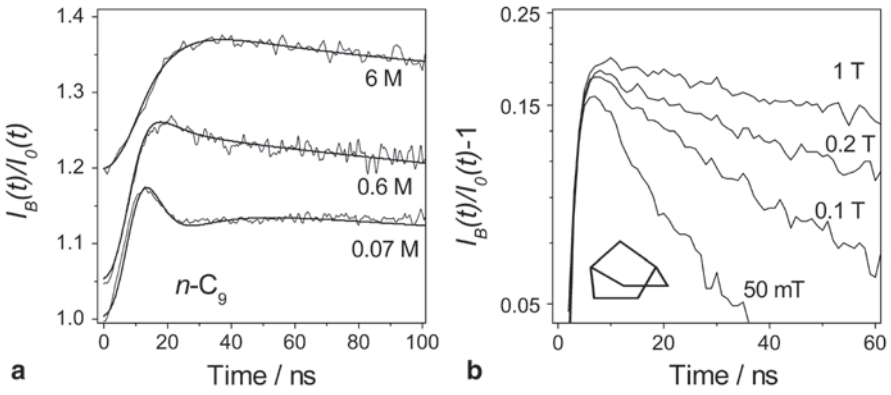

Fig. 17.14 TR MFE curves in solutions of *n*-nonane **a** in the field $B = 0.1$ T for various alkane concentrations (shown in the figure, adapted with permission from [119]. Copyright 2006, American Chemical Society) and 0.2 M norbornane **b** at varying magnetic field, T = 293 K, adapted with permission from [120]. Copyright 2006, American Chemical Society. The structure of the norbornane molecule is shown in the plot

If the RC has a considerable EPR spectrum width, the condition of the fast spectral exchange $(\sigma\tau)^2 \ll 1$ cannot be met for a realistic solution viscosity. In this case, the increasing rate of the exchange does not significantly affect the TR MFE curve. However, the spectral exchange contributes to spin-lattice relaxation. Figure 17.14b shows in semi-log coordinates TR MFE curves registered in *n*-hexane solution of norbornane at different magnetic fields [120]. The curve decay pattern is close to exponential in accordance with Eq. (17.13), so the dependence of the spin-lattice relaxation rate in the norbornane RC on the magnetic field and norbornane concentration can be determined. This, in turn, allows estimating the rate of reaction (17.15). Since the HFC in norbornane RC is determined by four equivalent protons (a(4H) ≈ 6.4 mT), the spin evolution can be calculated exactly [42] taking into account the reaction of charge transfer for any exchange rate. A comparison with the exact solution demonstrated that the Redfield theory of paramagnetic relaxation can be used even in weak magnetic fields at a low spectral exchange rate.

Irreversible Reactions Involving Geminate Radical Ions In OD EPR the effect of a reaction involving geminate radical ions can be successfully observed if the initial radical ion and the final reaction product have resolved and sufficiently different spectra. For example, the reaction of RC dimerization was thus observed [100, 121]. The estimation of the rate constant of a reaction in OD EPR or FDMR experiment is not very accurate. Other techniques can estimate it with a relatively high accuracy, including through indirect information from the MARY spectrum.

A reaction resulting in the formation of a new radical ion with a different EPR spectrum affects the dynamics of the spin state of the ensemble of spin-correlated RIPs. An appropriate TR MFE experiment then allows the real-time observation of the entire process. Figure 17.15a shows the transformation of TR MFE curves due to electron transfer from a molecule of 1,3-dimethyladamantane (DMAD) to the

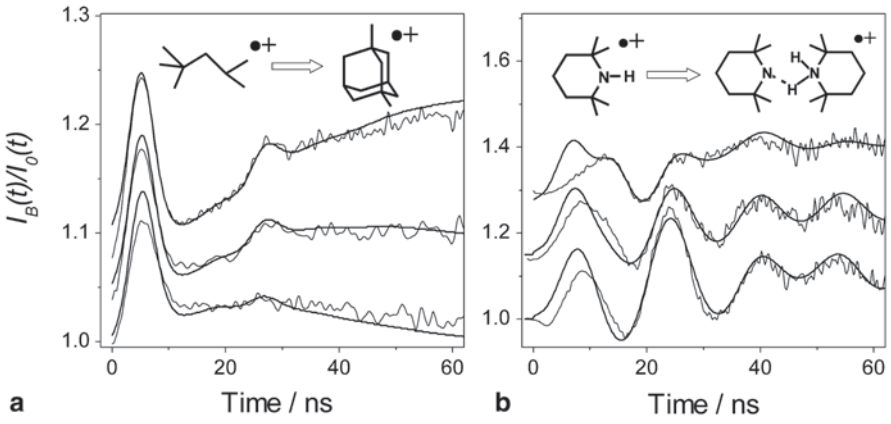

Fig. 17.15 Experimental (*noisy*) and calculated TR MFE curves recorded for: **a** *n*-hexane solutions of 0.1 M 2,2,4-trimethylpentane without (*curve 1)* and with 1 mM (*curve 2*) and 3 mM (*curve 3*) of 1,3-dimethyladamantane. The smooth lines show the results of calculation for reaction (17.16) at the rate constant of 1.5×10^{10} $M^{-1}s^{-1}$. Adapted with permission from [112]. Copyright 2012 American Chemical Society. **b** cyclohexane solutions (+30 μM *p*TP-d_{14}) of 3 mM (*curve 1*), 20 mM (*curve 2*), and 30 mM (*curve 3*) tetramethylpiperidine. The *smooth lines* show the results of calculation for reaction (17.17) at the rate constant of 6×10^9 $M^{-1}s^{-1}$. The curves are shifted vertically for convenience. Adapted from [123], Copyright 2008, Pleiades Publishing, Ltd

RC of 2,2,4-trimethylpentane (*iso*-C_8H_{18}) in hexane solution. The DMAD RC has a short spin-lattice relaxation time [122], so its formation in reaction

$$iso\text{-}C_8H_{18}{}^{+\bullet} + \text{DMAD} \rightarrow iso\text{-}C_8H_{18} + \text{DMAD}^{+\bullet} \qquad (17.16)$$

leads to a rapid loss of spin correlation in the radical ion pair $DMAD^{+\bullet}/p\text{-}TP^{-\bullet}$ that produces fluorescence upon recombination. In this case, the extra decay rate of the TR MFE due to the reaction (17.16) is approximately equal to the rate of the formation of the rapidly relaxing species.

More complicated for analysis is the transformation of the TR MFE curves in the case shown in Fig. 17.15b, when the reaction modifies the hyperfine structure of the radical ion. This was demonstrated using the example of the formation of a distonic complex of a RC with a molecule in irradiated solution of tetramethylpiperidine (TMPP) [123]:

$$\text{TMPP}^{+\bullet} + \text{TMPP} \rightarrow (\text{TMPP}^{\bullet} ... \text{TMPP}^{+}) \qquad (17.17)$$

The spin density distribution in this complex is similar to N-centered radicals.

The experimental TR MFE curves can be successfully described if the complex is considered to be formed from the RC with the rate constant of 6×10^9 $M^{-1}s^{-1}$, i.e., in a diffusion-controlled process involving molecular species. The process of the distonic complex formation was also detected in the OD EPR spectrum, although the rate constant of the reaction cannot be readily estimated from the spectrum.

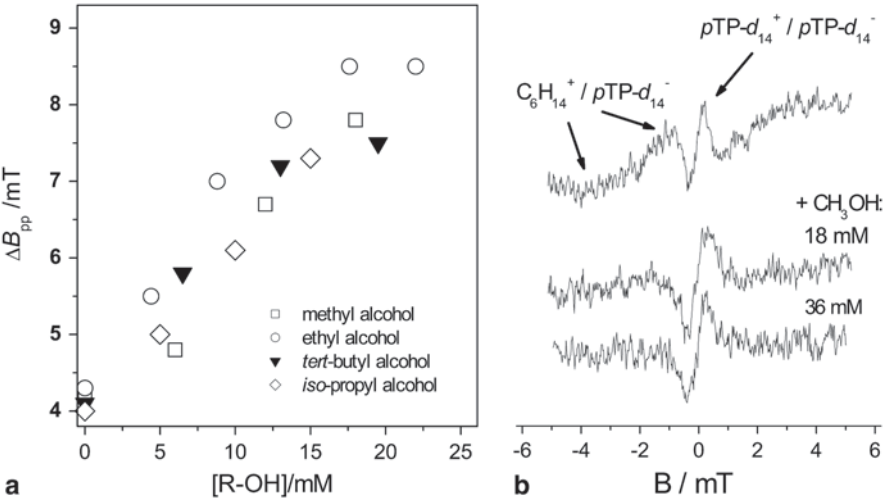

Fig. 17.16 **a** The dependence of the width of the zero-field MARY line in a solution of 10 mM hexafluorobenzene in *n*-hexane *vs.* the concentration of four different alcohols. The slope of the dependences corresponds to the rate constant of the deprotonation reaction $2 \div 3 \times 10^{10}$ $M^{-1}s^{-1}$. **b** A MARY spectrum for a solution of 2.5 mM *p*TP-d_{14} in *n*-hexane (the *upper curve*) and its change after adding methyl alcohol (the *lower two curves*) Adapted from [124]. Copyright 2003, with permission from Elsevier Science Ltd

Deprotonation of Alkane Radical Cations in MARY Information about the decay rate of the geminate radical ions can be obtained from the measurement of steady-state MFE as well. As mentioned above, the shortening of the lifetime (τ) of the pair increases the width (ΔB_{pp}) of the zero-field MARY line according to the relation for the Lorentz line contour $\Delta B_{pp}(\text{mT}) \approx 6.6/\tau$ (ns) known in the theory of EPR [60].

Such a shortening of the lifetime occurs, for example, during a reaction that separates the spin and the charge in one of the partners in a RIP. In irradiated alkanes such a reaction can be the proton transfer from an alkane RC ($RH^{+\bullet}$) to an aliphatic alcohol molecule, as Fig. 17.16a shows.

In refs [124, 125] it was shown that addition of an alcohol to a solution of hexafluorobenzene (C_6F_6) in *n*-alkane (*n*-C_6 to *n*-C_{10}) broadened the zero field MARY line proportionally to alcohol concentration in the range of up to ~20 mM, which is the threshold of alcohol association in alkane. From the analysis of the obtained MARY spectra it was determined, which of the decay channels of the spin-correlated radical ion pair $RH^{+\bullet}/C_6F_6^{-\bullet}$ was responsible for this broadening. As an example, Fig. 17.16b shows how the addition of an alcohol to a solution of *p*TP-d_{14} in alkane (RH) suppresses the characteristic signal from the pair $RH^{+\bullet}/p\text{TP-}d_{14}^{-\bullet}$ leaving the signal from the other pair $p\text{TP-}d_{14}^{+\bullet}/p\text{TP-}d_{14}^{-\bullet}$ unaffected. In this experiment it was established that there is no interaction between the radical anion in the pair and the alcohol molecule. As a result, in ref [124] it was concluded that a proton is transferred from the RC of a linear alkane to a monomeric molecule of an aliphatic alcohol with a diffusion-controlled rate.

17.6 Concluding Remarks

The methods of Optically Detected EPR, Time-Resolved Magnetic Field Effect, and MARY spectroscopy discussed in this chapter open new possibilities for registration and systematic investigation of radical ions in irradiated liquid solutions. Although invoking fluorescence for the detection, they can provide information on the radical ions of compounds exhibiting no luminescence. The methods are based on exploiting the spin correlation in the radical ion pairs generated in solution. This lends them sensitivity to the local track structure on the hitherto unexplored scale between a single pair and the entire path of high energy particles.

The methods have a very high sensitivity to the radical ions and open access to radical ions at the nanosecond time scale at their extremely low steady state concentrations in the irradiated sample. The method of OD EPR directly yields the CW EPR spectra of the radical ions of the pair partners. The method of TR MFE provides the time-resolved picture of the evolution of the spin state of the radical ion pairs, with simulations yielding the EPR spectral parameters. MARY spectroscopy proved to be a helpful indicatory express technique to estimate the width of the EPR spectra and the lifetimes of short-lived radical ions.

An advantage of the method of OD EPR is the conventional presentation of the spectrum and the simplicity of its interpretation. Furthermore, as opposed to time-resolved methods, both CW OD EPR and MARY spectroscopy do not require luminophores with short luminescence lifetime. On the other hand, the major advantage of TR MFE is its ability to directly determine relaxation times in a wide range of magnetic fields in addition to HFC and *g*-values, as well as the possibility to follow the transformations of a radical ion at the nanosecond time scale.

Regarding the most interesting results provided as examples in this chapter, we first of all mention the registration of radical ions in solutions, which either could not be detected by other techniques, or the very formation of which under irradiation was under question. Other interesting application fields for these methods include the study of intramolecular conformational transitions and the formation of intermolecular complexes of short-lived radical ions, the study of the processes of degenerate electron exchange, the study of the peculiarities of spin relaxation of these elusive species. It is clear that the potential of these methods by now has been anything but exhausted.

Acknowledgments The work was supported by the Council for Grants of the President of the Russian Federation for State Support of Leading Scientific Schools (Grant NSh-5744.2014.3).

References

1. Crookes W (1879) On the illumination of lines of molecular pressure, and the trajectory of molecules. Phil Trans Royal Soc Lond 170:135–164
2. Röntgen WC (1895) Über eine neue Art von Strahlen. Vorläufige Mitteilung. In: Aus den Sitzungsberichten der Würzburger Physik-Medic Ges Würzburg, pp 132–141

3. Becquerel H (1896) Sur les radiations invisibles émises par les corps phosphorescents, vol 22. Comptes rendus de l'Académie des sciences, Paris, pp 501–503
4. Child CD (1913) LXXVIII. Line spectrum from uncharged molecules. Phil Mag (Ser 6) 26:906–911
5. Merritt E (1915) Luminescence. Phys Rev 5:319–334
6. Marshall LC (1929) The recombination of ions and electrons in gases. Phys Rev 34:618–634
7. Morrow T, Salmon GA, Frankevich EL (1968) Effect of an electric field on the radiation induced fluorescence from solutions of aromatic hydrocarbons in cyclohexane. Nature 219:481–482
8. Dainton FS, Salmon GA, Morrow T, Thompson GF (1968) The formation of excited states on pulse radiolysis of organic solutions. Chem Commun 6:326–328
9. Brocklehurst B (1969) Formation of excited states by recombining organic ions. Nature 221:921–923
10. Brocklehurst B, Dixon RS, Gardy EM et al (1974) The effect of a magnetic field on the singlet/triplet ratio in geminate ion recombination. Chem Phys Lett 28:361–363
11. Brocklehurst B (1976) Magnetic field effect on the pulse shape of scintillations due to geminate recombination of ion pairs. Chem Phys Lett 44:245–248
12. Klein J, Voltz R (1976) Time-resolved optical detection of coherent spin motion for organic-radical-ion pairs in solution. Phys Rev Lett 36:1214–1217
13. Anisimov OA, Bizyaev VL, Lukzen et al (1983) The induction of quantum beats by hyperfine interactions in radical-ion pair recombination. Chem Phys Lett 101:131–135
14. Veselov AV, Melekhov VI, Anisimov OA, Molin YN (1987) The induction of quantum beats by the Δg mechanism in radical ion pair recombination. Chem Phys Lett 136:263–266
15. Grigoryants VM, Tadjikov BM, Usov OM, Molin YN (1995) Phase shift of quantum oscillations in the recombination luminescence of spin-correlated radical ion pairs. Chem Phys Lett 246:392–398
16. Veselov AV, Anisimov OA, Molin YN (1991) Time-resolved single-photon counting technique in radiolysis of hydrocarbons. In: Tabata Y (ed) Pulse radiolysis. CRC, Boston, pp 27–51
17. Anisimov OA, Grigoryants VM, Kiyanov SV et al (1982) Influence of magnetic field on recombination fluorescence in nonpolar solutions of hexafluorobenzene. Theor Exp Chem 18:256–261
18. Sukhenko SA, Purtov PA, Salikhov KM (1983) Proyavlenie peresecheniya urovney radical'nyh par v magnitnyh effektah I effektah himicheskoy polarizatsii yader (The manifestation of energy level intersection for radical-pair spins in magnetic effects and in the effects of magnetic nuclear polarization. In Russian). Khim Fiz 1:21−27
19. Anisimov OA, Grigoryants VM, Molchanov VK, Molin YN (1979) Optical detection of ESR absorption of short-lived ion-radical pairs produced in solution by ionizing radiation. Chem Phys Lett 66:265–268
20. Anisimov OA, Grigoryants VM, Molin YN (1979) Observation of hyperfine structure in the optical detection of the EPR spectrum of short-lived ion-radical pairs in a liquid. JETP Lett 30:555–557
21. Trifunac AD, Smith JP (1980) Optically detected time resolved EPR of radical ion pairs in pulse radiolysis of liquids. Chem Phys Lett 73:94–97
22. Molin YN, Anisimov OA (1983) Optical detection OD ESR spectra of short-lived ion-radical pairs in spurs under radiolysis. Radiat Phys Chem 21:77–82
23. Veselov AV, Bizyaev VL, Melekhov VI et al (1989) Detection of solvent holes by the method of quantum beats in recombination luminescence. Radiat Phys Chem 34:567–573
24. Trifunac AD, Werst DW (1991) Study of radical cations by time-resolved magnetic resonance. In: Lund A, Shiotani M (eds) Radical ionic systems. Kluwer, Dodrecht, pp 195–229
25. Werst DW, Bakker MG, Trifunac AD (1990) The fate of alkane radical cations in liquid and solid hydrocarbons. Time-resolved fluorescence detected magnetic resonance. J Am Chem Soc 112:40–50

26. Freeman GR (1987) Ionization and charge separation in irradiated materials. In: Freeman GR (ed) Kinetics of nonhomogeneous processes. Wiley, New York, pp 19–87
27. LaVerne JA, Brocklehurst B (1996) Magnetic field effects on the solute luminescence of alkane solutions irradiated with heavy ions. J Phys Chem 100:1682–1688
28. Holroyd RA, Preses JM, Hanson JC (1997) Excited singlet-state yields in hydrocarbon liquids exposed to X-rays. J Phys Chem A 101:6931–6935
29. Anishchik SV, Usov OM, Anisimov OA, Molin YN (1998) Study of a fraction of spin-correlated pairs in radiation spurs by the methods of time-resolved magnetic field effects and quantum beats. Radiat Phys Chem 51:31–36
30. Baker GJ, Brocklehurst B, Hayes M et al (1989) Ion-recombination luminescence in alkanes excited by synchrotron radiation in the range 10-40 eV. Chem Phys Lett 161:327–331
31. Brocklehurst B (1992) Model calculation on hydrocarbon radiolysis. Part 1—spin correlation effects in pure alkanes. J Chem Soc Faraday Trans 88:167–175
32. Lozovoy VV, Anishchik SV, Medvedev NN et al (1990) Monte Carlo modelling of radical ion recombination in multiparticle tracks. Chem Phys Lett 167:122–128
33. Borovkov VI, Velizhanin KA (2007) Experimental and computer simulation study of delayed fluorescence decay from irradiated *n*-dodecane solutions of TMPD. Radiat Phys Chem 76:998–1010
34. Salikhov KM, Molin YN, Sagdeev RZ, Buchachenko AL (1984) Spin polarization and magnetic effects in chemical reactions. Elsevier, Amsterdam
35. Steiner UE, Ulrich T (1989) Magnetic field effects in chemical kinetics and related phenomena. Chem Rev 89:51–147
36. Brocklehurst B (2002) Magnetic fields and radical reactions: Recent developments and their role in nature. Chem Soc Rev 31:301–311
37. Hayashi H (2004) Introduction to dynamic spin chemistry: magnetic field effects on chemical and biochemical reactions. World Scientific, Singapore
38. Bagryansky VA, Borovkov VI, Molin YN (2007) Quantum beats in radical pairs. Russ Chem Rev 76:493–506
39. Brocklehurst B (1973) An electron-tunnelling model for recombination of aromatic hydrocarbon radical ions in non-polar solvents. Chem Phys 2:6–18
40. Schulten K, Wolynes PG (1978) Semiclassical description of electron spin motion in radical including the effect of electron hopping. J Chem Phys 68:3292–3297
41. Stass DV, Lukzen NN, Tadjikov BM et al (1995) Ion-molecular charge-transfer reactions of hexafluorobenzene and *cis*-decalin in nonpolar solutions studied by linewidth broadening in MARY spectra. Chem Phys Lett 243:533–539
42. Bagryansky VA, Borovkov VI, Molin YN (2004) Spectroscopic capabilities of the time-resolved magnetic field effect technique as illustrated in the study of hexamethylethane radical cation in liquid hexane. Phys Chem Chem Phys 6:924–928
43. Bagryansky VA, Usov OM, Borovkov VI et al (2000) Quantum beats in recombination of spin-correlated radical ion pairs with equivalent protons. Chem Phys 255:237–245
44. Bagryansky VA, Ivanov KL, Borovkov VI et al (2005) Spin evolution of radical pairs with radicals containing two groups of equivalent magnetic nuclei. J Chem Phys 122(22):224503
45. Bagryansky VA, Borovkov VI, Molin YN (2002) Singlet-triplet oscillations of spin-correlated radical pairs due to the Larmor precession in low magnetic field. Mol Phys 100:1071–1078
46. Bagryansky VA, Usov OM, Lukzen NN et al (1997) Spin relaxation parameters in recombining radical ion pair (diphenylsulfide-d_{10}^{+})/(*p*-terphenyl-d_{14}^{-}) obtained by OD ESR and quantum beats techniques. Appl Magn Reson 12:505–512
47. Brocklehurst B (1985) Spin correlation effects in radiolysis. Int Rev Phys Chem 4:279–306
48. Bagryansky VA, Borovkov VI, Molin YN et al (1997) Quantum beats in the recombination of radical ion pairs caused by hyperfine interaction in radical anions. Mendeleev Commun 4:132–133

49. Stass DV, Lukzen NN, Tadjikov BM, Molin YN (1995) Manifestation of quantum coherence upon recombination of radical ion pairs in weak magnetic fields. Systems with non-equivalent nuclei. Chem Phys Lett 233:444–450
50. Rodgers CT (2009) Magnetic field effects in chemical systems. Pure Appl Chem 81:19–43
51. Timmel CR, Henbest KB (2004) A study of spin chemistry in weak magnetic fields. Phil Trans R Soc Lond A 362:2573–2589
52. Toropov YV, Sviridenko FB, Stass DV et al (2000) Influence of geminate recombination kinetics on the shape of low field MARY line. Chem Phys 253:231–240
53. Timmel CR, Till U, Brocklehurst B et al (1998) Effects of weak magnetic fields on free radical recombination reactions. Mol Phys 95:71–89
54. Tadjikov BM, Stass DV, Molin YN (1996) MARY-detected ESR spectra of radical ions in liquid solutions for systems with crossing Zeeman levels. Chem Phys Lett 260:529–532
55. Kalneus EV, Kipriyanov AA Jr, Purtov PA et al (2006) Specific MARY spectrum from radical anion of pentafluorobenzene. Appl Magn Reson 30:549–554
56. Kalneus EV, Stass DV, Molin YN (2005) Typical applications of MARY spectroscopy: radical ions of substituted benzenes. Appl Magn Reson 28:213–229
57. Stass DV, Anishchik SV, Verkhovlyuk VN (2011) Coherent spin control of radiation-generated radical ion pairs in liquid alkanes. In: Stass DV, Feldman VI (eds) Selectivity, control, and fine tuning in high-energy chemistry. Research Signpost, Kerala, pp 143–189
58. Weller A, Nolting F, Staerk H (1983) A quantitative interpretation of the magnetic field effect on hyperfine-coupling-induced triplet formation from radical ion pairs. Chem Phys Lett 96:24–27
59. Justinek M, Grampp G, Landgraf S et al (2004) Electron self-exchange kinetics determined by MARY spectroscopy: theory and experiment. J Am Chem Soc 126:5635–5646
60. Slichter CP (1990) Principles of magnetic resonance. Springer, Berlin
61. Saik VO, Ostafin AE, Lipsky S (1995) Magnetic field effects on recombination fluorescence in liquid *iso*-octane. J Chem Phys 103:7347–7358
62. Lersch W, Michel-Beyerle ME (1983) Magnetic field effects on the recombination of radical ions in reaction centers of photosynthetic bacteria. Chem Phys 78:115–126
63. Hoff AJ, Gast P, van der Vos R et al (1993) Magnetic field effects: MARY, MIMS and MODS. Z Phys Chem 180(1-2):175–192
64. Batchelor SN, McLauchlan KA, Shkrob IA (1992) Reaction yield detected magnetic resonance in exciplex systems: I. B_0 and B_1 spectra. Mol Phys 75:501–529
65. Doktorov AB, Anisimov OA, Burshtein AI, Molin YN (1982) Theory of optically detected magnetic resonance spectra of radical pairs. Chem Phys 71:1–8
66. Saik VO, Lukzen NN, Grigoryants VM et al (1984) Ion-molecular charge transfer as studied by the method of optically detected ESR of radical pairs. Chem Phys 84:421–430
67. Morozov VA, Doktorov AB (1991) Theory of multiquantum optically detected ESR spectra of radical pairs. I. General theory. Resonances in parallel radio-frequency field. Chem Phys 153:313–331
68. Lukzen NN, Saik VO, Anisimov OA et al (1985) Saturation of optically detected ESR spectra: Its relationship with kinetic and relaxation parameters of recombining radical-ion pairs. Chem Phys Lett 118:125–129
69. Koptyug AV, Saik VO, Anisimov OA et al (1989) Spin-locking in concentration-narrowed OD ESR spectra. Chem Phys 138:173–178
70. Anishchik SV, Grigoryants VM, Shebolaev IV et al (1989) Impulsny rentgenovsky fluorimetr s nanosecundnym rasresheniem (Pulse X-ray fluorimeter with the nanosecond resolution. In Russian). Prib Tech Exper 4:74–76
71. Anisimov OA (1991) Ion pairs in liquids. In: Lund A, Shiotani M (eds) Radical ionic systems. Kluwer, Dordrecht, pp 285–309
72. Trifunac AD, Bartels DM, Werst DW (1991) Time-resolved magnetic resonance study. In: Tabata Y (ed) Pulse radiolysis, CRC, Boca Raton, pp 53–75
73. Trifunac AD, Werst DW (1991) Study of radical cations by time-resolved magnetic resonance. In: Lund A, Shiotani M (eds) Radical ionic systems. Kluwer, Dordrecht, pp 195–229

74. Shkrob IA, Trifunac AD (1997) Spin and time-resolved magnetic resonance in radiation chemistry. Recent development and perspectives. Radiat Phys Chem 50:227–243
75. Sergey NV, Verkhovlyuk VN, Kalneus EV et al (2012) Registration of radical anions of Al, Ga, In *tris*-8-oxyquinolinates by magnetosensitive and spectrally resolved recombination luminescence in benzene solutions. Chem Phys Lett 552:32–37
76. Martini IB, Barthel ER, Schwartz BJ (2000) Mechanisms of the ultrafast production and recombination of solvated electrons in weakly polar fluids: comparison of multiphoton ionization and detachment via the charge-transfer-to-solvent transition of Na^- in THF. J Chem Phys 113:11245–11257
77. Borovkov VI, Ivanishko IS (2013) Measurement of the relative mobility of geminate ions in ethereal solutions of aromatic compounds using the fluorescence response of the solutions to pulsed irradiation. J Phys Chem B 117:15122−15130
78. Werst DW (1996) Self-exchange reactions of radical anions in *n*-hexane. Chem Phys Lett 251:315–322
79. Bagryansky VA, Borovkov VI, Molin YN (1998) Quantum beats in the recombination of radical ion pairs caused by hyperfine interaction in radical anions. Chem Phys Lett 295:230–236
80. Bagryansky VA, Molin YN, Egorov MP, Nefedov OM (1998) The first experimental detection, by OD ESR spectroscopy, of radical anions of siloles and germoles bearing hydrogen and chlorine substituents attached to heteroatom. Mendeleev Comm 6:236–237
81. Steingarts VD, Kobrina LS, Bilkis II, Starichenko VF (1991) Himiya polyftorarenov: Mehanizm reakciy, intermediaty (Chemistry of polyfluoroarenes: reaction mechanisms, intermediates. In Russian). Nauka, Novosibirsk
82. Hasegawa A, Itagaki Y, Shiotani M (1997) EPR spectra and structure of the radical cations of fluorinated benzenes. J Chem Soc Perkin Trans 2(9):1625–1632
83. Schastnev PV, Shchegoleva LN (1995) Molecular distortions in ionic and excited states. CRS, Boca Raton
84. Lozovoy VV, Grigoryants VM, Anisimov OA et al (1987) The HFI parameters and structure of radical-anions of substituted tetra- and pentafluorobensenes. Theory and experiment (OD ESR). Chem Phys 112:463–471
85. Barlukova MM, Beregovaya IV, Vysotsky VP et al (2005) Intramolecular dynamics of 1,2,3-trifluorobenzene radical anions as studied by OD ESR and quantum-chemical methods. J Phys Chem A 109:4404–4409
86. Blinkova SV, Shchegoleva LN, Beregovaya IV et al (2011) Intramolecular dynamics of the 1,2,4-trifluorobenzene radical anion: an optically detected EPR and quantum chemistry study. Appl Magn Reson 41:229–238
87. Yim MB, Wood DE (1976) Free radicals in an adamantane matrix. XII. EPR and INDO study of σ*-π* crossover in fluorinated benzene anions. J Am Chem Soc 98:2053–2059
88. Das MR, Wagner SB, Freed JH (1970) ESR relaxation studies on orbitally degenerate free radicals. II. J Chem Phys 52:5404–5417
89. Kalneus EV, Stass DV, Ivanov KL, Molin YN (2006) A MARY study of radical anions of fluorinated benzenes. Mol Phys 104:1751–1763
90. Blinkova SV, Vyushkova MM, Shchegoleva LN et al (2013) Isuchenie structurnyh osobennostey anion-radicala 1,3,5-triftorbenzola metodami OD EPR i kvantovoy himii (Study of 1,3,5-trifluorebenzene radical anion structure by means of OD EPR and quantum chemistry). Russ Chem Bull 11:2311–2316
91. de Haas MP, Warman JM, Infelta PP et al (1975) The direct observation of a highly mobile positive ion in nanosecond pulse irradiated liquid cyclohexane. Chem Phys Lett 31:382–386
92. Shkrob IA, Sauer MC Jr, Trifunac AD (2001) Radiation chemistry of organic liquids: saturated hydrocarbons. In: Jonah CD, Rao BSM (eds) Radiation chemistry. Present studies and future trends. Elsevier, Amsterdam, pp 175–221
93. Borovkov VI, Usov OM, Kobzeva TV et al (2002) Highly mobile primary radical cations (holes) in irradiated cyclooctane. Dokl Phys Chem 384:97–100

94. Usov OM, Stass DV, Tadjikov BM et al (1997) Highly mobile solvent holes in viscous squalane solutions as detected by quantum beats and MARY spectroscopy techniques. J Phys Chem A 111:7711–7717
95. Desrosiers MF, Trifunac AD (1985) Observation of transient cyclohexene and 1,4-cyclohexadiene radical cations. Time-resolved fluorescence detected magnetic resonance. Chem Phys Lett 118:441–443
96. Werst DW, Desrosiers MF, Trifunac AD (1987) Olefin radical cations in pulse radiolysis of hydrocarbons. Time-resolved fluorescence-detected magnetic resonance. Chem Phys Lett 133:201–206
97. Lefkowitz SM, Trifunac AD (1984) Time-resolved fluorescence-detected magnetic resonance and fluorescence studies of trialkylamines irradiated by pulse radiolysis in alkane solvents. J Phys Chem 88:77–81
98. Vyushkova MM, Bagryansky VA, Molin YN (2010) Application of optically detected EPR to study the stability of sterically hindered amine radical cations to proton transfer reaction. Appl Magn Reson 38:39–49
99. Grigoryants VM, Anisimov OA, Molin YN (1982) Study of the radical-cations of triethylamine and benzene derivatives by the optical detection of the EPR spectra of radical-ion pairs. J Struct Chem 23:327–333
100. Saik VO, Anisimov OA, Lozovoy VV, Molin YN (1985) Fast reaction involving radical cations during their geminate recombination as studied by the OD ESR method. Z Naturforsch 40a:239–245
101. Toriyama K (1991) ESR studies on cation radicals of saturated hydrocarbons. In: Lund A, Shiotani M (eds) Radical ionic systems. Kluwer, Dodrecht, pp 99–124
102. Shiotani M, Lindgren M, Ohta N et al (1991) Radical cations of cyclohexanes alkyl-substituted on one carbon: An ESR study of the Jahn-Teller distorted HOMO of cyclohexane. J Chem Soc Perkin Trans 2(5):711–719
103. Lindgren M, Shiotani M (1991) ESR studies of radical cations of cycloalkanes and saturated heterocycles. In: Lund A, Shiotani M (eds) Radical ionic systems. Kluwer, Dodrecht, pp 125–150
104. Melekhov VI, Anisimov OA, Sjoqvist L, Lund A (1990) The electronic structure of *cis*- and *trans*-decalin radical cations in halocarbon matrices: An ESR and MNDO study. Chem Phys Lett 174:95–102
105. Mehnert R (1991) Radical cations in pulse radiolysis. In: Lund A, Shiotani M (eds) Radical ionic systems. Kluwer, Dodrecht, pp 231–284
106. Tagawa S, Hayashi N, Yoshida Y et al (1989) Pulse radiolysis studies on liquid alkanes and related polymers. Radiat Phys Chem 34:503–511
107. Veselov AV, Bizyaev VL, Melekhov VI et al (1989) Detection of solvent holes by the method of quantum beats in recombination luminescence. Radiat Phys Chem 34:567–573
108. Borovkov VI, Bagryansky VA, Yeletskikh IV, Molin YN (2002) Radical cations of *n*-alkanes in irradiated solutions as studied by time resolved magnetic field effects. Mol Phys 100:1379–1384
109. Ichikawa T, Shiotani M, Ohta N, Katsumata S (1989) ESR and optical studies of solute n-alkane cations formed in.gamma.-irradiated n-pentane and n-hexane matrixes. J Phys Chem 93:3826–3831
110. Kowalewski J, Liljefors T (1979) On the relationship between the potential barrier and the activation energy for the internal rotation of a methyl group. Chem Phys Lett 64:170–174
111. Borovkov VI, Potashov PA, Shchegoleva LN et al (2007) Radical cations of branched alkanes as observed in irradiated solutions by the method of time-resolved magnetic field effect. J Phys Chem A 111:5839−5844
112. Potashov PA, Borovkov VI, Shchegoleva LN et al (2012) Radical cations of branched alkanes in solutions: Time-resolved magnetic field effect and quantum chemical studies. J Phys Chem A 116:3110−3117
113. Shkrob IA, Liu AD, Sauer MC et al (1998) Reversible hole trapping in liquid cyclohexane. J Phys Chem B 102:3371−3378

114. Borovkov VI, Molin YN (2004) Paramagnetic relaxation of cyclohexane radical cation in solution as measured by the method of time-resolved magnetic field effect. Phys Chem Chem Phys 6:2119–2124
115. Borovkov VI, Beregovaya IV, Shchegoleva LN et al (2012) Radical ions with nearly degenerate ground state: Correlation between the rate of spin-lattice relaxation and the structure of adiabatic potential energy surface. J Chem Phys 137:104305
116. Borovkov VI, Bagryansky VA, Molin YN et al (2003) Detection of radical cations of Group 14 element organometallics in alkane solutions using the method of time-resolved magnetic field effect. Phys Chem Chem Phys 5:2027–2033
117. Borovkov VI, Potashov PA, V. A. Bagryansky et al (2008) The study of radical cations of Me_3C-$SiMe_3$ and Me_3C-$GeMe_3$ in alkane solutions using the method of time-resolved magnetic field effect and DFT calculations. Chem Phys Lett 465:307–310
118. Iley J (1995) ESR of organogermanium, organotin and organolead radicals. In: Patai S (ed) The chemistry of organic germanium, tin and lead compounds. Wiley, pp 267–289
119. Borovkov VI, Gritsan NP, Yeletskikh IV et al (2006) Degenerate electron exchange reaction of *n*-alkane radical cations in solution. J Phys Chem A 110:12752–12759
120. Borovkov VI, Ivanov KL, Bagryansky VA, Molin YN (2006) Longitudinal electron spin relaxation induced by degenerate electron exchange as studied by time-resolved magnetic field effects. J Phys Chem A 110:4622–4628
121. Werst DW (1992) Radical cation complexes formed by π-lone pair interactions. J Phys Chem 96:3640–3646
122. Borovkov VI, Molin YN (2004) Paramagnetic relaxation of adamantane radical cation in solution. Chem Phys Lett 398:422–426
123. Vyushkova MM, Borovkov VI, Shchegoleva LN et al (2008) Unusual proton-transfer complex between the 2,2,6,6-tetramethylpiperidine radical cation and neutral molecule. Dokl Phys Chem 420(2):125–127
124. Stass DV, Sviridenko FB, Molin YN (2003) Magnetic field effect study of solvent hole deprotonation in X-irradiated liquid *n*-alkanes. Radiat Phys Chem 67:207–210
125. Sviridenko FB, Stass DV, Molin YN (2003) Study of interaction of aliphatic alcohols with primary radical cations of *n*-alkanes using MARY spectroscopy. Mol Phys 101:1839–1850